Hyperpolarized Magnetic Resonance

Lecture Notes

Benno Meier

April 19, 2023

Colophon
This document was typeset with the help of KOMA-Script and LaTeX using the kaobook class.
The source code of this book's template is available at:
https://github.com/fmarotta/kaobook

Publisher
First printed in March 2022

Contents

The Signal and the Noise 1

1.1 The Main Ideas

The objective of hyperpolarization is to increase the sensitivity of magnetic resonance by polarizing or aligning the spins to a degree that is *above* its thermal equilibrium value.

In this lecture we will first learn how to calculate the nuclear and electron spin polarization using the Boltzmann distribution. For experts in magnetic resonance, we will then calculate the same quantity using the spin density matrix. Knowledge of the polarization enables us to calculate the magnetization. The precessing magnetization gives rise to a voltage in the NMR coil, and this voltage is called the signal.

The polarization is by no means the only factor that determines the sensitivity of magnetic resonance. Indeed, a state of hyperpolarization can often be achieved only at the expense of analyte concentration or throughput, which adversely affects sensitivity.

In this lecture, we will learn

- how to calculate the polarization at thermal equilibrium
- how to calculate the magnetization for a given polarization
- how to calculate the induced voltage in the RF coil
- how to calculate the Signal-to-Noise Ratio (SNR) per unit time.

At the end of this lecture, you will be able to

1.2 The Polarization

The term describes the "net" alignment of spins in NMR and EPR. Since only the aligned spins give rise to the NMR signal, the signal is directly proportional to the polarization. This lecture series is about "Hyper-Polarization", that is about achieving a state of "higher than normal" polarization. As we will see soon, the potential to do so is huge.

1.2.1 The Nuclear Zeeman Interaction

In both the EPR and the NMR spin systems that we will discuss in this lecture the coupling between the spin and the external magnetic field is the dominant interaction. This coupling is called . For a classic magnetic moment we have

$$E = -\boldsymbol{\mu}\mathbf{B}. \tag{1.1}$$

Nuclear magnetic resonance is based on the fact that many nuclei have both a magnetic moment $\boldsymbol{\mu}$, and an angular momentum $\boldsymbol{J}$. The two quantities are parallel vectors, and we write

$$\boldsymbol{\mu} = \gamma \boldsymbol{J}. \tag{1.2}$$

Herein γ is the gyromagnetic ratio, a quantity that depends on the nucleus. $\boldsymbol{J}$ is an angular momentum operator. In magnetic resonance, we prefer to work with *dimensionless* angular momentum poperators $\boldsymbol{I}$ with

$$\hbar \boldsymbol{I} = \boldsymbol{J}. \tag{1.3}$$

$\boldsymbol{I}$ is a vector of operators, i.e. $\boldsymbol{I} = (\hat{I}_x, \hat{I}_y, \hat{I}_z)$.

Much like earth's magnetic field aligns the magnetic moment of a compass needle,[1] a magnetic field tends to align nuclear spins.

1: Note that without friction the compass needle would oscillate about the earth's field indefinitely, just like a swing without friction would swing indefinitely about earth's gravitational field. Also in NMR we need friction processes to achieve alignment, and these are known as T_1 processes.

The energy of the interaction, using Equations (1) and (2) is

$$E = -\boldsymbol{\mu B} \tag{1.4}$$

Now we choose to apply the magnetic field along the z-axis, i.e. $\boldsymbol{B} = (0, 0, B_0)$, and we obtain

$$E = -\gamma \hbar \hat{I}_z B_0 \tag{1.5}$$

Note that the above equation does not give a value (in Joule), but rather it specifies an operator. The operator that describes the energy structure of the system is called the Hamiltonian in quantum mechanics, and written, in this case, as

$$\mathscr{H} = -\gamma \hat{I}_z B_0, \tag{1.6}$$

Note that we have dropped $\hbar$ - we follow the usual convention in NMR and express energies as angular frequencies. In NMR we deal with systems with discrete energy levels, and the spin operators can be represented as matrices. The eigenvectors of the Hamiltonian matrix correspond to the stationary states of the system, and the eigenvalues to their respective energies.

In order to find the energy values, we need to find the eigenvalues of $\hat{I}_z$. To do so, we have to calculate the *matrix representation* of $\hat{I}_z$. This can only be done with respect to a defined basis. We denote the spin states with

$$\left|I, m_{-1/2}\right\rangle = |1/2, -1/2\rangle = |-1/2\rangle = |-\rangle = |\beta\rangle \tag{1.7}$$
$$\left|I, m_{+1/2}\right\rangle = |1/2, 1/2\rangle = |1/2\rangle = |+\rangle = |\alpha\rangle \tag{1.8}$$

The spin states form an orthonormal basis. This means that

$$\langle\alpha|\alpha\rangle = \langle\beta|\beta\rangle = 1. \tag{1.9}$$
$$\langle\alpha|\beta\rangle = \langle\beta|\alpha\rangle = 0. \tag{1.10}$$

Note that the above expression describe the orthogonality of (normalized) eigenvectors with respect to the scalar product.

The notation $|I, m\rangle$ is the general notation for a Ket for a single spin. With the symbol $|1/2, -1/2\rangle$, we have simply inserted the value for a spin $1/2$ in the $-1/2$ state. There are nuclei with higher spin. For example,

deuterium has total spin $I = 1$, and to give its eigenstate with $m_z = 0$, we would write $|1, 0\rangle$. Note that m_z takes values $-I, -I+1, ..., I$, so that for a spin one nucleus like deuterium we have three eigenstates.

Recall from quantum mechanics that $\hat{I}_z$ extracts the projection quantum number m_z. The matrix representation of $\hat{I}_z$ for a single spin-1/2 particle is

$$\begin{pmatrix} \langle\alpha|\hat{I}_z|\alpha\rangle & \langle\alpha|\hat{I}_z|\beta\rangle \\ \langle\beta|\hat{I}_z|\alpha\rangle & \langle\beta|\hat{I}_z|\beta\rangle \end{pmatrix} = \begin{pmatrix} 1/2 & 0 \\ 0 & -1/2 \end{pmatrix} \tag{1.11}$$

We see that $\hat{I}_z$ is already diagonal, with eigenvalues $1/2$ and $-1/2$. The energy levels of the spin are therefore

$$E = \pm\frac{1}{2}\gamma B_0. \tag{1.12}$$

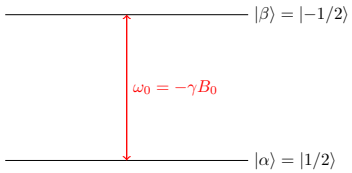

Figure 1.1: Spitting of Zeeman levels in an external magnetic field. The figure is correct for nuclei with a positive gyromagnetic ratio, for which the Larmor frequency is negative. These are, for example ^{1}H, ^{13}C, ^{14}N, but not ^{15}N, which has a negative gyromagnetic ratio.

We see that the splitting between the two states depends on the nuclear gyromagnetic ratio γ and is proportional the magnetic field B_0.

Note that the nuclear Zeeman interaction by itself is *isotropic*, i.e. the splitting does not depend on the orientation of the magnetic field.

The electron Zeeman interaction

As we will see in more detail soon, the electron Zeeman interaction depends on the orientation of the magnetic field with respect to the so-called g-tensor. For the purpose of calculating polarizations, we can ignore this dependence, and use the free electron g-factor as an approximation, i.e. $g \approx 2.0023$. The gyromagnetic ratio of a free electron is $\gamma_S = g\mu_B$, where μ_B is the Bohr magneton.

Note that the anisotropy of the electron Zeeman interaction is analogous to the chemical shift anisotropy in NMR, but it may be of the order of unity, where as chemical shifts in NMR are specified in ppm.

1.2.2 The Boltzmann Distribution

The polarization P of the spins is defined as follows

$$P = \frac{p_{|\alpha\rangle} - p_{|\beta\rangle}}{p_{|\alpha\rangle} + p_{|\beta\rangle}} = p_{|\alpha\rangle} - p_{|\beta\rangle} = 1 - 2p_{|\beta\rangle} \tag{1.13}$$

Herein, $p_{|\alpha\rangle}$ and $p_{|\beta\rangle}$ are the fractions of spins in the $|\alpha\rangle$ and $|\beta\rangle$ states respectively. Note that all spins are either in the $|\alpha\rangle$ or in the $|\beta\rangle$ state, i.e. $p_{|\alpha\rangle} + p_{|\beta\rangle} = 1$.

We have not treated relaxation, and so we have no mechanism which would cause a spin to transition, e.g., from $|\alpha\rangle$ to $|\beta\rangle$. Nevertheless, we know that spin systems (usually) achieve a thermal equilibrium. In doing so, they exchange energy with their surrounding, which is called the *lattice*. The time constant for this process is the *spin-lattice* relaxation time

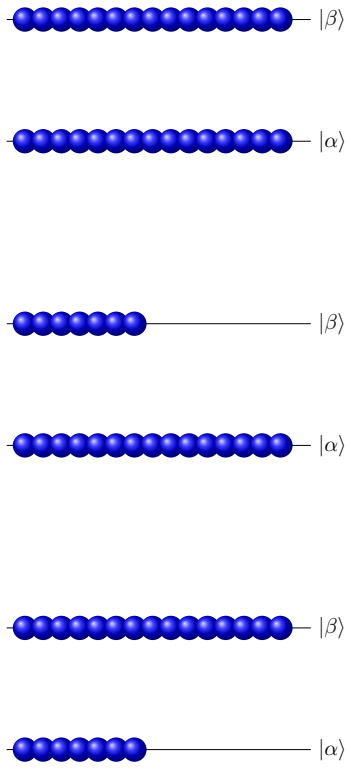

Figure 1.2: Spin state populations corresponding to zero polarization (top), positive hyperpolarization (middle), and negative hyperpolarization (bottom).

constant T_1. After a few T_1s, the system achieves equilibrium with the lattice, and the ratio of the populations is then given by

$$\frac{p_{|\beta\rangle}}{p_{|\alpha\rangle}} = \exp\left(-\frac{\hbar\gamma B}{kT}\right) \tag{1.14}$$

where T is the lattice (e.g. sample) temperature.

Solving the above equation for $p_{|\beta\rangle}$ gives

$$p_{|\beta\rangle} = (1 - p_{|\beta\rangle}) \exp\left(-\frac{\hbar\gamma B}{kT}\right) \tag{1.15}$$

$$p_{|\beta\rangle}\left(1 + \exp\left(-\frac{\hbar\gamma B}{kT}\right)\right) = \exp\left(-\frac{\hbar\gamma B}{kT}\right) \tag{1.16}$$

$$p_{|\beta\rangle} = \frac{\exp\left(-\frac{\hbar\gamma B}{kT}\right)}{1 + \exp\left(-\frac{\hbar\gamma B}{kT}\right)} \tag{1.17}$$

$$= \frac{1}{1 + \exp\left(+\frac{\hbar\gamma B}{kT}\right)} \tag{1.18}$$

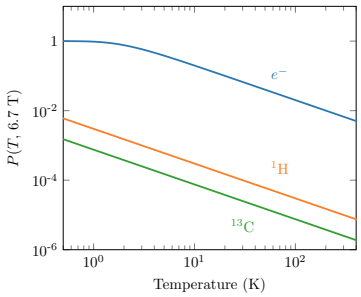

Figure 1.3: Thermal equilibrium polarization for the electron (blue), ^{1}H (orange) and ^{13}C at a field of 6.7 Tesla

Insertion into Eq. (1.13), and using the relation $\tanh(x) = 1 - \frac{2}{1+\exp(2x)}$ yields

$$P = 1 - 2p_{|\beta\rangle} = 1 - \frac{2}{1 + \exp\left(+\frac{2\hbar\gamma B}{2kT}\right)} = \tanh\left(\frac{\hbar\gamma B}{2kT}\right), \tag{1.19}$$

With this expression we can calculate the thermal equilibrium polarization for any spin 1/2 nucleus, as well as the electron for any field and temperature. The result is shown in Fig. 1.3 for a magnetic field of 6.7 Tesla. Note the exceedingly small polarization of the nuclear spins at ambient temperature (approximately 10^{-5} at 300 Kelvin). The electron has a much larger gyromagnetic ratio, and a correspondingly higher polarization. At temperatures of the order of 1 Kelvin, electron spins become fully polarized.

[1]: Overhauser (1953), 'Polarization of Nuclei in Metals'

[2]: Carver et al. (1953), 'Polarization of Nuclear Spins in Metals'

[3]: Slichter (2010), 'The Discovery and Demonstration of Dynamic Nuclear Polarization-A Personal and Historical Account'

Albert Overhauser realised in 1952 [1], that in metals the large polarization of conduction electrons could be transfered to nuclear spins by saturating the electron spin transition. Charlie Slichter thought Al's prediction to be correct, and, together with his student Tom Carver, conceived and conducted an experiment that showed a dramatic increase in the NMR signal intensity of ^{7}Li in lithium metal. They published their work in August 1953 [2], only months after Overhauser had published his ideas.

An inspiring account of the "birth of hyperpolarization" has been given by Slichter [3].

Since Overhauser's discovery, several other hyperpolarization mechanisms have been discovered, one of them () also by Carver. However, the term dynamic nuclear polarization was taken, and is reserverd for hyperpolarization mechanisms in which *electrons* are the source

of hyperpolarization.

Equation (1.19) suggests a straight forward way to achieve near unity polarization, namely to apply a field of a few Tesla, and cool the sample down to Millikelvin temperatures. This approach has actually been explored and is called brute-force hyperpolarization [4]. The major problem with brute-force polarization is that spin-lattice relaxation becomes exceedingly long at temperatures below 1 K, and a state of high polarization may not be achieved at all. The relaxation time may be shortened using paramagnetic dopants, but the polarization levels achieved in this way are still lower than what can be achieved with DNP.

[4]: Hirsch et al. (2015), 'Brute-Force Hyperpolarization for NMR and MRI'

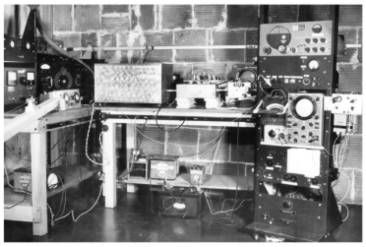

Figure 1.4: The first DNP Spectrometer. Reproduced from Ref. [3]

Under ambient conditions, we have $\hbar\gamma B \ll kT$, or $x \ll 1$. We may then use the expansion $\tanh(x) \approx x$, and the polarization for a spin 1/2 evaluates to[2]

$$P \approx \frac{\hbar\gamma B}{2kT}. \tag{1.20}$$

This is the high-temperature approximation in NMR. It applies for all spin 1/2 nuclei at practical fields (< 100 Tesla) and temperatures (> 1 Kelvin), but not for electron spins at 1 Kelvin and 5 Tesla.

1.2.3 Polarization and the Density Matrix

We conclude this section by discussing the polarization for spins > 1/2. In principle, one can use (1.14) to solve also for a higher spin. There is however a more elegant way which is part of the standard NMR toolbox. Namely we will calculate the expectation value of $\hat{I}_z$. For a fully polarized spin system we have $P = 1$, and the expecation value of $\hat{I}_z$ equals 1/2. For a system with full negative polarization, the exepectation value equals $-1/2$.

We define the polarization for an arbitrary spin I as

$$P = \frac{1}{I}\left\langle \hat{I}_z \right\rangle \tag{1.21}$$

The polarization defined in this way assumes values from -1 to $+1$ for any spin I. It should be noted however that for spins > 1/2, this definition has to be used with care. Consider, as an example an ensemble of ^{14}N spins, which are all in the $|1;0\rangle$ state. Although this is a highly-ordered, pure state, it has no magnetization, and the above definition ascribes it zero polarization.

The expectation value of an operator can be calculated using the *density operator*. The thermal equilibrium density operator is written as

$$\hat{\rho} = \frac{1}{Z}\exp\left(-\frac{\hbar\mathcal{H}}{kT}\right) = \frac{1}{Z}\exp\left(+\frac{\hbar\gamma\hat{I}_z B_0}{kT}\right) \tag{1.22}$$

Herein, Z is the partition sum,

$$Z = \sum_j \exp(-E_j/kT) = \sum_{m_z=-I}^{I} \exp(+\hbar\gamma B m_z/kT) \tag{1.23}$$

$$= \sum_{m_z=-I}^{I} \exp(\tilde{B} m_z), \tag{1.24}$$

where we have introduced the dimensionless quantity $\tilde{B} = \hbar\gamma B/kT$ to shorten the notation.

We choose the Zeeman basis in which the Hamiltonian is diagonal. Therefore, the matrix representation of $\hat{\rho}$ is also diagonal, with entries $\exp\left(\tilde{B} m_z\right)$. To calculate the expectation value of $\hat{I}_z$, we have to calculate the trace over $\hat{\rho}\hat{I}_z$. For a spin-1/2 we have

$$\begin{aligned}
P &= \frac{1}{\frac{1}{2}}\mathrm{Tr}\left(\hat{\rho}\hat{I}_z\right) = \frac{2}{Z}\mathrm{Tr}\left(\begin{pmatrix}\exp(\tilde{B}\cdot(1/2)) & 0\\ 0 & \exp(\tilde{B}\cdot(-1/2))\end{pmatrix}\begin{pmatrix}1/2 & 0\\ 0 & -1/2\end{pmatrix}\right)\\
&= \frac{\exp(\tilde{B}\cdot(1/2)) - \exp(-\tilde{B}\cdot(1/2))}{\exp(-\tilde{B}\cdot(1/2)) + \exp(\tilde{B}(1/2))}\\
&= \frac{\exp(\tilde{B}\cdot(1/2)) + \exp(-\tilde{B}\cdot(1/2)) - 2\exp(-\tilde{B}\cdot(1/2))}{\exp(-\tilde{B}\cdot(1/2)) + \exp(+\tilde{B}(1/2))}\\
&= 1 - \frac{2\exp(-\tilde{B}\cdot(1/2))}{\exp(-\tilde{B}\cdot(1/2)) + \exp(+\tilde{B}(1/2))}\\
&= 1 - \frac{2}{1+\exp(\tilde{B})} = 1 - \frac{2}{1+\exp(2\tilde{B}/2)} = \tanh(\tilde{B}/2)
\end{aligned}$$

which is the familiar result.

For a spin 1 we get, in complete analogy,

$$\begin{aligned}
P &= \frac{1}{1}\mathrm{Tr}\left(\hat{\rho}\hat{I}_z\right)\\
&= \frac{1}{Z}\mathrm{Tr}\left(\begin{pmatrix}\exp(-\tilde{B}) & 0 & 0\\ 0 & \exp(0) & 0\\ 0 & 0 & \exp(+\tilde{B})\end{pmatrix}\begin{pmatrix}1 & 0 & 0\\ 0 & 0 & 0\\ 0 & 0 & -1\end{pmatrix}\right)\\
&= \frac{\sum_{m=-1}^{1} m_z \exp(\tilde{B} m_z)}{\sum_{m=-I}^{I} \exp(\tilde{B} m_z)}
\end{aligned}$$

For an arbitrary spin, the polarization is

$$P = \frac{1}{I}\frac{\sum_{m=-I}^{I} m_z \exp(\tilde{B} m_z)}{\sum_{m=-I}^{I} \exp(\tilde{B} m_z)} \tag{1.25}$$

We can use the above expression to derive a simple expression for the polarization of a nucleus with *arbitrary spin I* in the high-temperature limit, using the expansion $\exp(x) \approx 1 + x$. Then we have

$$P \approx \frac{1}{I}\frac{\sum_{m=-I}^{I} m_z(1 + \tilde{B} m_z)}{\sum_{m=-I}^{I} 1 + x} \tag{1.26}$$

In the nominator the sum over m_z is zero, and in the denominator we can ignore x. Then, using the relation

$$\sum_{m=-I}^{I} m^2 = \frac{I(I+1)(2I+1)}{3} \tag{1.27}$$

we have

$$P \approx \frac{1}{I}\frac{\tilde{B}\sum_{m=-I}^{I} m_z^2}{(2I+1)} = \frac{1}{I}\frac{\tilde{B}I(I+1)(2I+1)}{3(2I+1)} = \frac{\tilde{B}(I+1)}{3} \tag{1.28}$$

Note that this expression corresponds to (1.20) for a spin $I = 1/2$.

1.3 The Magnetization

The polarization is a so-called *intensive* qunatity. It does not change when we incraese the amount of sample in our detector. The NMR signal of course is an *extensive* quantity, it does scale with the number of spins in the detector.

The NMR signal is induced in a coil by the precessing magnetization. The magnetization is usually defined as magnetic moment per unit volume, with the unit A/m. The magnetic moment is the expectation value of $\boldsymbol{\mu}$, and we denote the spin density (the number of spins N per volume V) with $n = N/V$. Then we have

$$M = n\langle\mu\rangle = n\gamma\hbar\langle\boldsymbol{I}\rangle\,. \tag{1.29}$$

We assume that the magnetic field is again applied along the z axis.[3] Then, there will be only a magnetization along z, given by

$$M_z = n\gamma\hbar\left\langle\hat{I}_z\right\rangle = n\gamma\hbar\mathrm{Tr}(\hat{\rho}\hat{I}_z) \tag{1.30}$$

Now we have already calculated the expectation value of $\hat{I}_z$, and we may write it as $\left\langle\hat{I}_z\right\rangle = IP$, where P is given by Eq. (1.25).

The general result for the magnetization is therefore

$$M_z = n\gamma\hbar IP, \tag{1.31}$$

where P is given by equation (1.25).

In the case of a spin 1/2 in the high-field limit this may be written, using equation (1.19), as

$$M_z = n\gamma\hbar\frac{1}{2}\tanh(\tilde{B}/2). \tag{1.32}$$

In the case of an arbitrary spin in the high-temperature limit we use (1.28), and have

$$M_z = n\gamma\hbar I\frac{\tilde{B}(I+1)}{3} = \frac{n\gamma^2\hbar^2 BI(I+1)}{3kT} \tag{1.33}$$

This equation is known as the Curie law.

3: A radio-frequency (RF) pulse is of course requried to generate the transverse magnetization that gives rise to the NMR signal. We assume that the RF pulse is a perfect 90 degree pulse, so that the transverse magnetization *after* the pulse will equal the longitudinal magnetization M_z *before* the pulse.

1.4 The NMR Signal

While it is difficult to make accurate predictions for signal intensities (and signal-to-noise ratio) from first principles, it is straightforward to estimate the order of magnitude of these quantities.

1.4.1 The induced voltage

Following a 90 degree or $\pi/2$ - pulse, the magnetization will precess about the magnetic field with a frequency ω. Faraday's law of induction states that the voltage induced in a coil with N turns by a changing flux Φ is

$$V_S = -N\frac{\mathrm{d}\Phi}{\mathrm{d}t}. \tag{1.34}$$

The flux is given as the magnetic field B flowing through the coil, multiplied with its cross-section A. The magnetic field in turn is given by $B = \mu_0 M$. If we assume M to precess according to $M = M_z \sin(\omega t)$, we have

$$V_S = -NA\mu_0\omega M_z \cos(\omega t) \tag{1.35}$$

The induced signal scales as $\gamma^3 B_0^2$. We might be tempted to use lots of turns to achieve a larger voltage. However, the coil geometry also dictates the noise level.

The Principle of Reciprocity

An alternative way to estimate the voltage has been given by Hoult in his now classic paper [5]. Clearly, if a given current generates a larger magnetic field at a certain point in space, then a precessing magnetic moment at that point will induce a larger voltage in the same coil. This is the principle of reciprocity.

[5]: Hoult et al. (1976), 'The Signal-To-Noise Ratio of the Nuclear Magnetic Resonance Experiment'

To derive the principle of reciprocity we need the Biot-Savart Law, which gives the magnetic field produced by a current I running along a wire C. We assume the current to be constant, and rewrite the law for later convenience:

$$\boldsymbol{B}_1(\boldsymbol{r}) = \frac{\mu_0}{4\pi}\int_C \frac{I\mathrm{d}\boldsymbol{l}\times\boldsymbol{r}}{r^3} = -I\frac{\mu_0}{4\pi}\int_C \frac{\boldsymbol{r}\times\mathrm{d}\boldsymbol{l}}{r^3} \tag{1.36}$$

We furthermore need the vector potential of a magnetic dipole,

$$\boldsymbol{A}(\boldsymbol{r}') = \frac{\mu_0}{4\pi}\frac{\boldsymbol{m}\times\boldsymbol{r}'}{r'^3}, \tag{1.37}$$

and the fact that the magnetic field due to $\boldsymbol{A}$ is given by

$$\boldsymbol{B}(\boldsymbol{r}) = \mathrm{rot}\boldsymbol{A}. \tag{1.38}$$

Now we use Faraday's law of induction

$$V = -\frac{\mathrm{d}\Phi}{\mathrm{d}t} = -\frac{\mathrm{d}}{\mathrm{d}t}\iint_{\mathrm{Area}} \boldsymbol{B}\cdot\mathrm{d}\boldsymbol{a}, \tag{1.39}$$

where $\mathrm{d}\boldsymbol{a}$ is the surface element. Now we insert Equation (1.38), use

Stokes' theorem, insert the expression for $\boldsymbol{A}$, and rearange using the cyclic relation $(\boldsymbol{a} \times \boldsymbol{b}) \cdot \boldsymbol{c} = (\boldsymbol{b} \times \boldsymbol{c}) \cdot \boldsymbol{a}$:

$$V = -\frac{\mathrm{d}}{\mathrm{d}t} \iint_{\text{Area}} \mathrm{rot}\boldsymbol{A} \cdot \mathrm{d}\boldsymbol{a} = -\frac{\mathrm{d}}{\mathrm{d}t} \int_C \boldsymbol{A} \cdot \mathrm{d}\boldsymbol{l} \tag{1.40}$$

$$= -\frac{\mathrm{d}}{\mathrm{d}t} \frac{\mu_0}{4\pi} \int_C \frac{\boldsymbol{m} \times \boldsymbol{r}'}{r^3} \cdot \mathrm{d}\boldsymbol{l} = +\frac{\mathrm{d}}{\mathrm{d}t} \underbrace{\frac{\mu_0}{4\pi} \int_C \frac{\boldsymbol{r} \times \mathrm{d}\boldsymbol{l}}{r^3}}_{=-\boldsymbol{B}_1/I} \cdot \boldsymbol{m} \tag{1.41}$$

$$= -\frac{\mathrm{d}}{\mathrm{d}t} \frac{1}{I} \boldsymbol{B} \cdot \boldsymbol{m} \tag{1.42}$$

Note the relation $\boldsymbol{r}' = -\boldsymbol{r}$, since in the case of the Biot-Savart law we are looking away from the coil to the point of the magnetic moment, whereas in the case of the vector potential we are interested in the vector potential at the distance $\boldsymbol{r}'$ from the magnetic moment.[4]

4: Thanks to Mengjia He for spotting this error!

Now recall that magnetization is defined as magnetic moment per unit volume. Thus, to get the voltage for *all* magnetic moments, we replace the magnetic moment with the magnetization, and integrate over the volume.

$$V = -\frac{\mathrm{d}}{\mathrm{d}t} \frac{1}{I} \iiint \boldsymbol{B} \cdot \boldsymbol{M} \mathrm{d}V \tag{1.43}$$

This is the principle of reciprocity: The voltage induced in the coil by a precessing magnetic moment is the larger, the larger the magnetic field generated by the coil at the place of the precessing magnetic moment.

If the magnetization and the magnetic field are constant across the sample volume, and if the magnetization precesses in the transverse plane according to $M_x = M_0 \sin(\omega t)$, this simplifies to

$$V = -\frac{B_1}{I} \omega M_0 V_s \cos(\omega t) \tag{1.44}$$

Since a good detector will have a homogeneous B_1 accross the sample, it can be seen that the signal scales exactly as *magnetic field per current*.

It is frequently useful to estimate the strength of the B_1 field for a given circuit. Such an estimate has been given by Slichter [6].

[6]: Slichter (1990), 'Principles of Magnetic Resonance'

An inductor carrying a current I stores an energy

$$\frac{1}{2} L I^2. \tag{1.45}$$

But this energy is really the energy of the field that is produced by the current, so we may write

$$\frac{1}{2} L I^2 = \frac{1}{2} \iiint \boldsymbol{M}\boldsymbol{B} \mathrm{d}V = \frac{1}{2\mu_0} B^2 V_c \tag{1.46}$$

where we have assumed that the field is homogenoeus and contained in the coil with volume V_c.

In steady state, the power dissipated in the coil equals the power provided

by the RF amplifier. We therefore have

$$\frac{1}{2}RI^2 = P \quad I^2 = \frac{2P}{R}. \tag{1.47}$$

Substituting this into equation (1.46), we get

$$\frac{1}{2}\frac{L2P}{R} = \frac{1}{2\,\mu_0}B^2V_c. \tag{1.48}$$

Now we use the relation $Q = \omega L/R$, and solve for B:

$$B = \sqrt{\frac{QP2\mu_0}{\omega V_c}}. \tag{1.49}$$

Now the field generated by the coil is linearly polarized, and has to be decomposed into two circularly polarized fields, e.g.

$$B = B_1\exp(\mathrm{i}\omega t) + B_1\exp(-\mathrm{i}\omega t). \tag{1.50}$$

Therefore

$$B_1 = B/2 = \sqrt{\frac{\mu_0 QP}{2\omega V_c}}. \tag{1.51}$$

In this equation Q is readily measured by the width of the return loss spectrum 7 dB below the baseline [7].

[7]: Doty et al. (1988), 'Noise in High-Power, High-Frequency Double-Tuned Probes'

1.4.2 The noise

The electrons in the coil wire generate a noise voltage, which is known as Johnson or Nyquist noise [8]. The noise voltage is given by

$$V_N = \sqrt{4kTR\Delta f}. \tag{1.52}$$

[8]: Nyquist (1928), 'Thermal Agitation of Electric Charge in Conductors'

Here, Δf is the bandwidth over which the noise is measured, T is the coil's temperature, and R is its resistance. It can be seen that cooling the coil is a very good idea - it lowers the temperature *T and* the resistance R. Indeed, cryoprobes can give an approximately 4-fold increase in SNR.[9]

[9]: Kovacs et al. (2005), 'Cryogenically Cooled Probes-A Leap in Nmr Technology'

1.5 The Signal-to-Noise Ratio of the NMR Experiment

The Signal-to-Noise Ratio (SNR) of the NMR experiment is simply the ratio of the signal and the noise voltages. In practice, the SNR is lower, because the preamplifier adds a bit of *extra* noise to the signal. It is possible to increase the SNR by averaging more than one acquisitions. The NMR signal is the same in every acquisition, but the noise is different. When averaging, the SNR increases with the square-root of the number of acquisitons, or equivalently, with the square root of time.

It should be stressed that there are many ways to increase the SNR that do *not* rely on hyperpolarization. These range from adding paramagnetic impurities to increase the cycle time, to pulse sequences such as INEPT

that report on insensitive low-γ nuclei by exploiting their couplings to sensitive high-γ nuclei, to parallel acquisition. For a review of these techniques, see [10].

[10]: Kupče et al. (2021), 'Parallel Nuclear Magnetic Resonance Spectroscopy'

1.6 Concluding Remarks

In this lecture we have seen that the NMR signal is proportional to the nuclear spin polarization, and that the latter is very small. By contrast, the electron spin has a much larger polarization, and becomes almost fully polarized at low temperatures. We have already mentioned briefly that the large electron polarization can be transferred to nuclear spins. This transfer is known as dynamic nuclear polarization. The process of DNP can be carried out under static conditions at very low temperatures, which is the focus of this lecture series. It may also be combined with magic angle spinning to increase the sensitivity of solid-state NMR. Finally it may be carried out in solution, where it is referred to as Overhauser-DNP. In any case, to understand the process better, we need a refined understanding of the spectrum of electron spins as it is recorded in electron paramagnetic resonance (EPR). This is the topic of the following lecture.

The electrons attain a highly polarized state because the electron Zeeman interaction is much larger than the nuclear Zeeman interaction. Another large interaction that may be used to create a nearly pure spin states is the rotational splitting of hydrogen. The class of hyperpolarization technologies that employ the rotational splitting of hydrogen is known as parahydrogen-induced polarization (PHIP). We will briefly discuss PHIP towards the end of this lecture series.

1.7 Further Reading

Here I give a few additional references which have not been cited in the lecture.

- This lecture can be no substitute for a thorough introduction to central concepts of magnetic resonance, including angular momentum, spin operators and the density matrix. An excellent, detailed introduction to these topics has been given by Levitt [11].
- To read about the art of discerning signal and noise in disciplines outside NMR, such as meteorology, climate change, or financial markets, have a look at Silver's excellent book "The Signal and the Noise: The Art and Science of Prediction" [12].

1.8 Python

In this lecture we will be using Python for everything from evaluating simple expressions to setting up Hamiltonians and systems of differential equations.

You can use any other tool that does the job for you, but the tool should allow you to carry out matrix multiplication in a simple way.

If you choose to give Python a go, the Anaconda Python distribution[5] is a good start. On Linux systems you already have Python. On Windows, if you don't want to install anything, you can use WinPython [6]. Both Anaconda and WinPython come wiht a server for Jupyter notebooks and Jupyter lab.

5: Available from https://www.anaconda.com/products/distribution

6: Available from http://winpython.github.io/

Once you have python up and running, you can run

```
pip install spindata3
```

The spindata module stores the gyromagnetic ratios of all NMR active nuclei, and the electron. An example is shown below. The code below loads the numpy module (which stores π as np.pi), and the spindata module. The last line is a print statement that prints the given number dE / (2*np.pi*1e6) as a float with two digits after the decimal point. The code is best run inside a Jupyter Notebook.

```
# import numpy module
import numpy as np

# import spindata module
from spindata import gamma

# magnetic field in Tesla
B = 1

# calculate energy splitting
dE = gamma("1H")*B

print("{:.2f} MHz".format(dE / (2*np.pi*1e6))
```

For the electron use "E" instead of "1H".

Constants such as $\hbar$ and the Boltzmann constant k are made available in Python by running

```
from scipy.constants import hbar, k
```

1.9 Exercises

1. Give the matrix representation of $\hat{I}_z$ in the Zeeman basis for a spin $I = 3/2$. Do this first on paper, then create it in Python using the np.diag command, and finally create the matrix representation for an arbitrary half-integer or integer spin using a for loop.
2. Calculate the polarization of (i) free electron spins at 6.7 Tesla and 1 Kelvin, and (ii) ^{13}C at the same field, but at 300 Kelvin. What is the ratio of the two?
3. A hyperpolarization method supplies a bolus of liquid containing a molecule of interest with a polarization that is 10,000 times higher than the thermal equilibrium polarization in the magnet. However, the hyperpolarization method leads to a 20-fold dilution of the analyte. The hyperpolarization experiment can be run every hour, but the analyte has a short T_1 of 0.2 s, and the acquisition on the thermal equilibrium sample can be run every second. How do the SNRs of hyperpolarization and "brute-force" compare after 1 hour?

You find out that no one is using the spectrometer, and run the experiment for another 15 hours. How do the SNRs compare now?

4. The proton channel of your new 400 MHz probe has a Q of 200, and a coil volume of 0.5 mL. Calculate the B_1 and the duration of a $\pi/2$ pulse for an RF power of 50 W.

EPR I. The Electron Zeeman Interaction

2

2.1 The Main Ideas

In Dynamic Nuclear Polarization, polarization is transferred from electron spins to nuclear spins. This process depends critically on the properties of the electron spins. In the next two lectures we are not concerned with DNP (yet), but we want to understand the electron spin spectrum. Because the measurement technique is known as electron paramagnetic resonance (EPR), this spectrum is known as the EPR spectrum.

We will start with the simple case of Trityl, where the EPR spectrum is due to the Zeeman anisotropy.

Its Hamiltonian may be written as

$$\mathcal{H} = -\boldsymbol{B}\boldsymbol{\mu} = \mu_B \boldsymbol{B}\boldsymbol{g}\hat{\boldsymbol{S}} \tag{2.1}$$

Note that the scalar gyromagnetic ratio from NMR has been replaced with a $\boldsymbol{g}$-tensor. As a consequence, the strength of the Zeeman interaction depends on the orientation of the magnetic field with respect to the $\boldsymbol{g}$-tensor.

In this lecture, we will learn

- that the electron Zeeman interaction is anisotropic, and how this anisotropy influences the EPR spectrum in solids.
- how to write and diagonalize the Hamiltonian using the spin operators $\hat{S}_x$ and $\hat{S}_y$.
- what Kernel Density Estimates are, and how they may be used to calculate a powder spectrum.
- how rotations are used to transform entities from one reference frame to another.

At the end of this lecture, you will be able to calculate the EPR spectrum for trityl, and we will be in a good position to take on spin systems with more than one spin.

As an outlook, in the next lecture we will look at further interactions. We will then study the Hamiltonian of Tempo, where the electron spin couples to the spin-1 ^{14}N nuclear spin. To discuss this case, we need to introduce spin operators for more than one spin, and the concept of tensor rotations. The Hamiltonian of Tempo may be written as

$$\mathcal{H} = -\boldsymbol{B}\boldsymbol{\mu} = \mu_B \boldsymbol{B}\boldsymbol{g}\hat{\boldsymbol{S}} + \hat{\boldsymbol{S}}\boldsymbol{A}\hat{\boldsymbol{I}} \tag{2.2}$$

2.2 The Electron Zeeman Interaction

The electron Zeeman interaction is the interaction of an electron spin with a magnetic field, just like the nuclear Zeeman interaction is the

interaction of a nuclear spin with a magnetic field. There are however two most significant differences between the interactions.

The first difference is that the electron Zeeman interaction is *larger*. The electron spins used in DNP have g-values very close to those of a free electron spin, and - consequentially - the electron Zeeman interaction is 660 times larger than that of the proton. Consequentially, the resonance frequencies that we deal with in DNP are of the order of 100 GHz, and we need microwave transmitters to excite electron transitions, and microwave receivers if we want to detect the transitions directly.

There are techniques to measure the EPR transitions indirectly.

The second difference is that the electron Zeeman interaction is *anisotropic*. For radicals such as those used in DNP, this anisotropy can be as high as 0.5 %, and a dominant source of line broadening. For other radicals, the anisotropy can be of the order of unity.

Recall that in NMR the magnetic moment is given by $\boldsymbol{\mu} = +\gamma\hbar\boldsymbol{I}$, that is the spin and the magnetic moment are parallel for postive γ (and antiparallel for negative γ).

In contrast, the magnetic moment of an electron spin is[1]

$$\boldsymbol{\mu} = -\mu_B \boldsymbol{g} \hat{\boldsymbol{S}} \tag{2.3}$$

1: Note that there are different sign conventions in use in the EPR community. Here we follow Abragam and Bleaney, but see also Ref. [13].

Here, the quantity $\boldsymbol{g}$ is the $\boldsymbol{g}$-Tensor, which takes the form of a 3x3 matrix. The significance of $\boldsymbol{g}$ is that the interaction energy of the magnetic moment with the applied field now depends on the angle between the $\boldsymbol{g}$ tensor and the applied magnetic field. For the origin of the anisotropy we refer to the EPR introduction by Gunnar Jeschke.

https://ethz.ch/content/dam/ethz/special-interest/chab/physical-chemistry/epr-dam/documents/education/EPR_PCIV_compressed.pdf

The Zeeman interaction for the electron spin then is written in its most general form as

$$\mathcal{H} = -\boldsymbol{B}\boldsymbol{\mu} = \mu_B \boldsymbol{B} \boldsymbol{g} \hat{\boldsymbol{S}} \tag{2.4}$$

Note that because $\boldsymbol{g}$ is a matrix, the magnetic moment and the spin $\boldsymbol{S}$ are not necessarily parallel anymore. For example, the following $\boldsymbol{g}$-Tensor

$$\boldsymbol{g} = \begin{pmatrix} 6 & 0 & 0 \\ 0 & 6 & 0 \\ 0 & 0 & 2 \end{pmatrix} \tag{2.5}$$

gives a magnetic moment

$$\boldsymbol{\mu} = -\mu_B (6\hat{S}_x, 6\hat{S}_y, 2\hat{S}_z), \tag{2.6}$$

which is not parallel to $\hat{S}$ anymore.

The frame in which $\boldsymbol{g}$ has only diagonal elements (as in the example above) is called the principal axis frame (PAF) of the g-tensor.

$$\boldsymbol{g} = \begin{pmatrix} g_x & 0 & 0 \\ 0 & g_y & 0 \\ 0 & 0 & g_z \end{pmatrix} \tag{2.7}$$

For now, we choose our coordinate system to coincide with the PAF of the g-tensor. This tensor may be visualized as an ellipsoid. In its prinicpal axis frame, the values g_x, g_y, and g_z give the intersections of the ellipsoid with the respective axes.

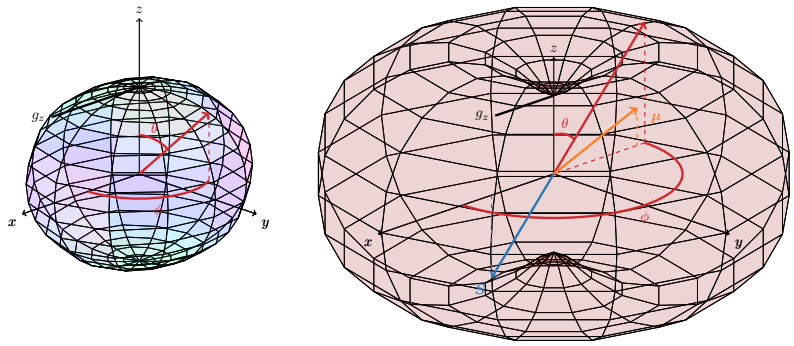

Figure 2.1: The electron Zeeman interaction for a Nitroxide radical (left, anisotropy exagerated 100-fold) and for Fe(III) (right, anisotropy to scale). The direction of the applied magnetic field may be specified using angles θ and ϕ, leading to an effective g-value which, for a given orientation, is given by the intersection of the $\boldsymbol{B}$ vector and the surface of the ellipsoid. For paramagnetic centers with a large anisotropy, the expectation value of the spin S (shown here with arbitrary scale) at thermal equilibrium points in the negative direction of the applied magnetic field). The magnetic moment μ associated with the spin S (again with arbitrary scale) is aligned with the magnetic field only for vanishing anisotropy. If the anisotropy is significant, as in the example on the right, μ instead appears tilted towards the xy-plane of the principal axis frame.

The direction of the magnetic field with respect to the $\boldsymbol{g}$-tensor may be specified using the spherical angles ϕ and θ, as shown in Fig. 2.1 (left).

The Hamiltonian may then in the PAF frame be written as

$$\mathcal{H}^{[\mathrm{PAF}]} = \mu_B B_0(\sin\theta\cos\phi, \sin\theta\sin\phi, \cos\theta)\begin{pmatrix} g_x & 0 & 0 \\ 0 & g_y & 0 \\ 0 & 0 & g_z \end{pmatrix}\begin{pmatrix} \hat{S}_x \\ \hat{S}_y \\ \hat{S}_z \end{pmatrix} \tag{2.8}$$

$$= \mu_B B_0(\sin\theta\cos\phi g_x\hat{S}_x + \sin\theta\sin\phi g_y\hat{S}_y + \cos\theta g_z\hat{S}_z) \tag{2.9}$$

The term in brackets gives the components of the spin in the PAF of the g tensor.

In order to find the energy levels of this Hamiltonian, we follow Abragam and Bleaney [14]. We introduce the direction cosines $l = \sin\theta\cos\phi$, $m = \sin\theta\sin\phi$ and $n = \cos\theta$, and we also introduce the rotated direction cosines l' with $gl' = g_x l$.

[14]: Abragam et al. (1970), *Electron Paramagnetic Resonance of Transition Ions*

We furthermore set

$$g = \sqrt{(g_x l)^2 + (g_y m)^2 + (g_z n)^2}. \tag{2.10}$$

Then the Hamiltonian may be written as

$$\mathcal{H} = g\mu_B B_0(l'\hat{S}_x + m'\hat{S}_y + n'\hat{S}_z), \tag{2.11}$$

and we have

$$l'^2 + m'^2 + n'^2 = \frac{g_x^2 l^2}{g^2} + \frac{g_y^2 m^2}{g^2} + \frac{g_z^2 n^2}{g^2} = 1. \tag{2.12}$$

The Hamiltonian has the same structure as that of a free spin with direction cosines l', m' and n', and an effective g-factor

$$g_{\mathrm{eff}} = \sqrt{(g_x l)^2 + (g_y m)^2 + (g_z n)^2}. \tag{2.13}$$

Its energy levels are therefore

$$E_i = \pm\frac{1}{2} g_{\text{eff}}(\phi, \theta)\mu_B B_0 \tag{2.14}$$

Direct Diagonalization of the Hamiltonian

We may also calculate the energy levels in a more "brute-force" way. To do so we need to recall a few more facts about spin operators (see Chapter 7 of [11] for a detailed review):

[11]: Levitt (2008), 'Spin Dynamics: Basics of Nuclear Magnetic Resonance'

$$\hat{S}_\pm = \hat{S}_x \pm \mathrm{i}\hat{S}_y \tag{2.15}$$

$$\hat{S}_x = \frac{1}{2}\left(\hat{S}_+ + \hat{S}_-\right) \tag{2.16}$$

$$\hat{S}_y = \frac{1}{2i}\left(\hat{S}_+ - \hat{S}_y\right) \tag{2.17}$$

The actions of $\hat{S}_\pm$ on a basis ket are

$$\hat{S}_+ |S, m_s\rangle = \sqrt{S(S+1) - m_s(m_s+1)}\,|S, m_s+1\rangle \tag{2.18}$$

$$\hat{S}_- |S, m_s\rangle = \sqrt{S(S+1) - m_s(m_s-1)}\,|S, m_s-1\rangle \tag{2.19}$$

$$\tag{2.20}$$

In particular for the electron we have $S = 1/2$ and $m_S = \pm 1/2$, and hence

$$\hat{S}_+ |\alpha\rangle = \hat{S}_+ \left|\frac{1}{2}; \frac{1}{2}\right\rangle = 0 \tag{2.21}$$

$$\hat{S}_+ |\beta\rangle = \hat{S}_+ \left|\frac{1}{2}; -\frac{1}{2}\right\rangle = \sqrt{\frac{1}{2}\frac{3}{2} - \left(-\frac{1}{2}\right)\left(\frac{1}{2}\right)} = \left|\frac{1}{2}; \frac{1}{2}\right\rangle = |\beta\rangle \tag{2.22}$$

and, by analogy

$$\hat{S}_- |\beta\rangle = 0, \hat{S}_- |\alpha\rangle = |\beta\rangle \tag{2.23}$$

Thus the matrix representations are

$$\left\langle \hat{S}_+ \right\rangle = \begin{pmatrix} \langle\alpha|\hat{S}_+|\alpha\rangle & \langle\alpha|\hat{S}_+|\beta\rangle \\ \langle\beta|\hat{S}_+|\alpha\rangle & \langle\beta|\hat{S}_+|\beta\rangle \end{pmatrix} = \begin{pmatrix} 0 & 1 \\ 0 & 0 \end{pmatrix} \tag{2.24}$$

$$\left\langle \hat{S}_- \right\rangle = \begin{pmatrix} 0 & 0 \\ 1 & 0 \end{pmatrix} \tag{2.25}$$

$$\left\langle \hat{S}_x \right\rangle = \frac{1}{2}\begin{pmatrix} 0 & 1 \\ 1 & 0 \end{pmatrix} \tag{2.26}$$

$$\left\langle \hat{S}_y \right\rangle = \frac{1}{2\mathrm{i}}\begin{pmatrix} 0 & 1 \\ -1 & 0 \end{pmatrix} \tag{2.27}$$

$$\left\langle \hat{S}_z \right\rangle = \frac{1}{2}\begin{pmatrix} 1 & 0 \\ 0 & -1 \end{pmatrix} \tag{2.28}$$

Now the Hamiltonian may be written (in the Zeeman basis, and using the directional cosines) as

$$\mathscr{H} = \frac{\mu_B B_0}{2}\begin{pmatrix} ng_z & lg_x - img_y \\ lg_x - img_y & -ng_z \end{pmatrix} \tag{2.29}$$

The eigenvalues of a 2x2 matrix

$$\begin{pmatrix} a & b \\ c & d \end{pmatrix}$$

are given by

$$\lambda_{1,2} = \frac{T}{2} \pm \sqrt{\frac{T^2}{4} - D}, \tag{2.30}$$

where $T = a + d$ is the trace and $D = ad - bc$ is the determinant. In our case we have $T = 0$ and $D = ad - bc = -n^2 g_z^2 - (l^2 g_x^2 - i^2 m^2 g_y^2)$ so

$$E_{1,2} = \frac{\mu_B B_0}{2} \lambda_{1,2} = \frac{\mu_B B_0}{2} \sqrt{-D} = \frac{\mu_B B_0}{2} \sqrt{n^2 g_z^2 + l^2 g_x^2 + m^2 g_y^2}. \tag{2.31}$$

The eigenvectors to the eigenvalues $\lambda_{1,2}$ are $(\lambda_{1,2} - d, c)$, and can be used to complete new basis functions:

$$\left|\phi_{1,2}\right\rangle = c' \left\{ (\lambda_{1,2} - d) \left|\alpha\right\rangle + c \left|\beta\right\rangle \right\}. \tag{2.32}$$

where $c' = 1/\sqrt{(\lambda_{1,2} - d)^2 + |c|^2}$ ensures normalization. We leave it as an exercise to show that the Hamiltonian $\mathcal{H}$ is diagonal in $\{\left|\phi_1\right\rangle, \left|\phi_2\right\rangle\}$.

Here, we have calculated the eigenvalues of the Hamiltonian by hand. However, the advantage of this approach is that it is readily extended to more complicated spin systems. We can always use a computer to calculate the Hamiltonian and find its eigenvalues without having to think too hard!

2.3 The EPR Spectrum

In liquid-state EPR of small molecules, if only the Zeeman interaction is present, the rapid tumbling of the molecule carrying the spin leads to an average process, and only a narrow resonance is observed at the average g-value $(g_x + g_y + g_z)/3$.

In the solid, such an averaging process is absent, and the resonance frequency of the spin depends on the orientation of its g-tensor with respect to the applied field. In glassy samples as we use them for DNP, all orientations occur with the same probability, and the EPR spectrum is an average of all these spectra. This average is called a powder spectrum [15].

To calculate the EPR spectrum $S(\omega)$, we vary the angles ϕ and θ, and calculate g_{eff}. Then we calculate the EPR spectrum for this particular orientation $S(\omega, \phi, \theta)$. The powder EPR spectrum is just the average over all these orientations:

$$S^{\text{Powder}}(\omega) = \frac{1}{4\pi} \iint S(\omega, \phi, \theta) \sin\theta \mathrm{d}\theta \mathrm{d}\phi, \tag{2.33}$$

where the term $\sin\theta$ reflects the decreasing probability for orientations with values of θ close to 0 and π, and the factor $1/(4\pi)$ ensures normalization.

If only g-anisotropy is present, it is possible (but not trivial) to derive an analytic solution for the powder spectrum (see for instance appendix I. of [6]). Such an approach however quickly becomes intractable if further interactions enter the Hamiltonian. We will therefore calculate the powder spectrum numerically. To do so, we use a technique from data analysis, called Kernel Density Estimates (KDE, see the excellent data analysis book by Janert [16] for details on this technique). We will also not calculate the EPR spectrum, but the spectrum of g values, $S(g)$, which gives the probability of finding a particular g value.

[6]: Slichter (1990), 'Principles of Magnetic Resonance'

[16]: Janert (2010), *Data Analysis with Open Source Tools*

We assign a kernel to every $g_{\text{eff}}(\phi, \theta)$-value that we encounter. The outcome of the procedure does not depend strongly on the choice of kernel K, so we choose a Gaussian one.

$$K(g_{\text{eff}}, g) = \frac{1}{\sqrt{2\pi\sigma^2}} \exp\left(-\frac{(g - g_{\text{eff}})^2}{2\pi\sigma^2}\right) \tag{2.34}$$

Note that in this expression g_{eff} is given by Eq. (2.13) and depends on ϕ and θ.

Now the g-spectrum can be calculated as

$$S(g) = \frac{1}{4\pi} \sum_{\phi_j} \sum_{\theta_k} K(g_{\text{eff}}(\theta_k, \phi_j), g) \sin(\theta_k) \Delta\phi \Delta\theta. \tag{2.35}$$

For example, if we partition ϕ into 100 values, we have $\phi_0 = 0 * 2\pi/100$, $\phi_1 = 1 * 2\pi/100$, $\Delta\phi = 2\pi/100$, and similar for θ.

We can get an EPR spectrum at a particular field, by transforming the g values to frequency values,

$$\nu = g * \mu_B B_0/\hbar \tag{2.36}$$

and plotting $S(g)$ vs. ν.

Now that we have the spectrum for a free paramagnetic centre, we need to have a look at other interactions. Crucially, we need to express all interactions in the same frame, and to do that we need to move from one frame to another. In other words, we need coordinate rotations.

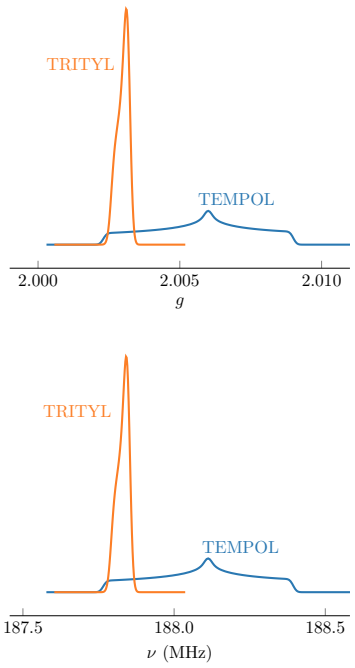

Figure 2.2: The EPR spectrum for Trityl and Tempol. The top view shows the spectrum of g-values, and the bottom view shows the corresponding EPR spectrum at a field of 6.7 Tesla. The hyperfine interaction is ignored for the time being.

2.4 Coordinate Rotations

Since the PAFs of the hyperfine and the Zeeman interaction may differ, we need to be able to express all interactions in the same frame. To see how this is done, we will now express the Hamiltonian in the lab frame.

There are various ways in which we can express our Hamiltonian in the lab frame. In general, the lab frame will be rotated with respect to the PAF frame, and such a rotation can be specified using a set of three so-called Euler angles α, β, γ. In the zyz convention, these have the following meaning>

1. first by an angle γ about the lab z-axis, (axis 3) and then
2. then rotate the rotated element by an angle β about the lab frame y-axis (axis 2).

3. finally rotate the twice rotated element by an angle α about the lab frame z axis (axis 3).

The rotation matrix for the first transformation is

$$R_3(\gamma) = \begin{pmatrix} \cos(\gamma) & \sin(\gamma) & 0 \\ -\sin(\gamma) & \cos(\gamma) & 0 \\ 0 & 0 & 1 \end{pmatrix} \tag{2.37}$$

The rotation matrix for the second transformation is

$$R_2(\beta) = \begin{pmatrix} \cos(\beta) & 0 & -\sin(\beta) \\ 0 & 1 & 0 \\ \sin(\beta) & 0 & \cos(\beta) \end{pmatrix} \tag{2.38}$$

The rotation matrix for the third transformation is

$$R_3(\alpha) = \begin{pmatrix} \cos(\alpha) & \sin(\alpha) & 0 \\ -\sin(\alpha) & \cos(\alpha) & 0 \\ 0 & 0 & 1 \end{pmatrix} \tag{2.39}$$

The rotation matrix of all three rotations combined (and using the zyz convention) is known as the Euler rotation matrix $\mathcal{R}$, with

$$\begin{aligned} \mathcal{R}(\alpha,\beta,\gamma) &= R_3(\alpha)R_2(\beta)R_3(\gamma) \\ &= \begin{pmatrix} -\sin(\alpha)\sin(\gamma)+\cos(\alpha)\cos(\beta)\cos(\gamma) & \sin(\alpha)\cos(\gamma)+\sin(\gamma)\cos(\alpha)\cos(\beta) & -\sin(\beta)\cos(\alpha) \\ -\sin(\alpha)\cos(\beta)\cos(\gamma)-\sin(\gamma)\cos(\alpha) & -\sin(\alpha)\sin(\gamma)\cos(\beta)+\cos(\alpha)\cos(\gamma) & \sin(\alpha)\sin(\beta) \\ \sin(\beta)\cos(\gamma) & \sin(\beta)\sin(\gamma) & \cos(\beta) \end{pmatrix} \end{aligned}$$

Since the magnetic field is applied along the lab z-axis, the final rotation about α is of no consequence to our interaction, and we can drop it, and we write $R = \mathcal{R}(0,\beta,\gamma)$.

In order to transform a vector to the new frame, we just apply the rotation matrix from the left:

$$\boldsymbol{S}^{[\mathrm{Lab}]} = R\boldsymbol{S}^{[\mathrm{PAF}]} \tag{2.40}$$

Then the result of the transformation for the spin $\boldsymbol{S}$ is

$$\begin{pmatrix} \hat{S}_x \\ \hat{S}_y \\ \hat{S}_z \end{pmatrix}^{[\mathrm{Lab}]} = \begin{pmatrix} \cos(\beta) & 0 & -\sin(\beta) \\ 0 & 1 & 0 \\ \sin(\beta) & 0 & \cos(\beta) \end{pmatrix} \begin{pmatrix} \cos(\gamma) & \sin(\gamma) & 0 \\ -\sin(\gamma) & \cos(\gamma) & 0 \\ 0 & 0 & 1 \end{pmatrix} \begin{pmatrix} \hat{S}_x \\ \hat{S}_y \\ \hat{S}_z \end{pmatrix} \tag{2.41}$$

$$= \begin{pmatrix} \hat{S}_x\cos(\gamma)\cos(\beta) + \hat{S}_y\sin(\gamma)\cos(\beta) - \hat{S}_z\sin(\beta) \\ -\hat{S}_x\sin(\gamma) + \hat{S}_y\cos(\gamma) \\ \hat{S}_x\sin(\beta)\cos(\gamma) + \hat{S}_y\sin(\gamma)\sin(\beta) + \hat{S}_z\cos(\beta) \end{pmatrix} \tag{2.42}$$

In order to transform a tensor to the new frame, we apply the *inverse* rotation from the right, and the rotation from the left. Note that the inverse of a rotation matrix is equal to its transpose.

$$\boldsymbol{g}^{[\mathrm{Lab}]} = R\boldsymbol{g}^{[\mathrm{PAF}]}R^{-1} \tag{2.43}$$

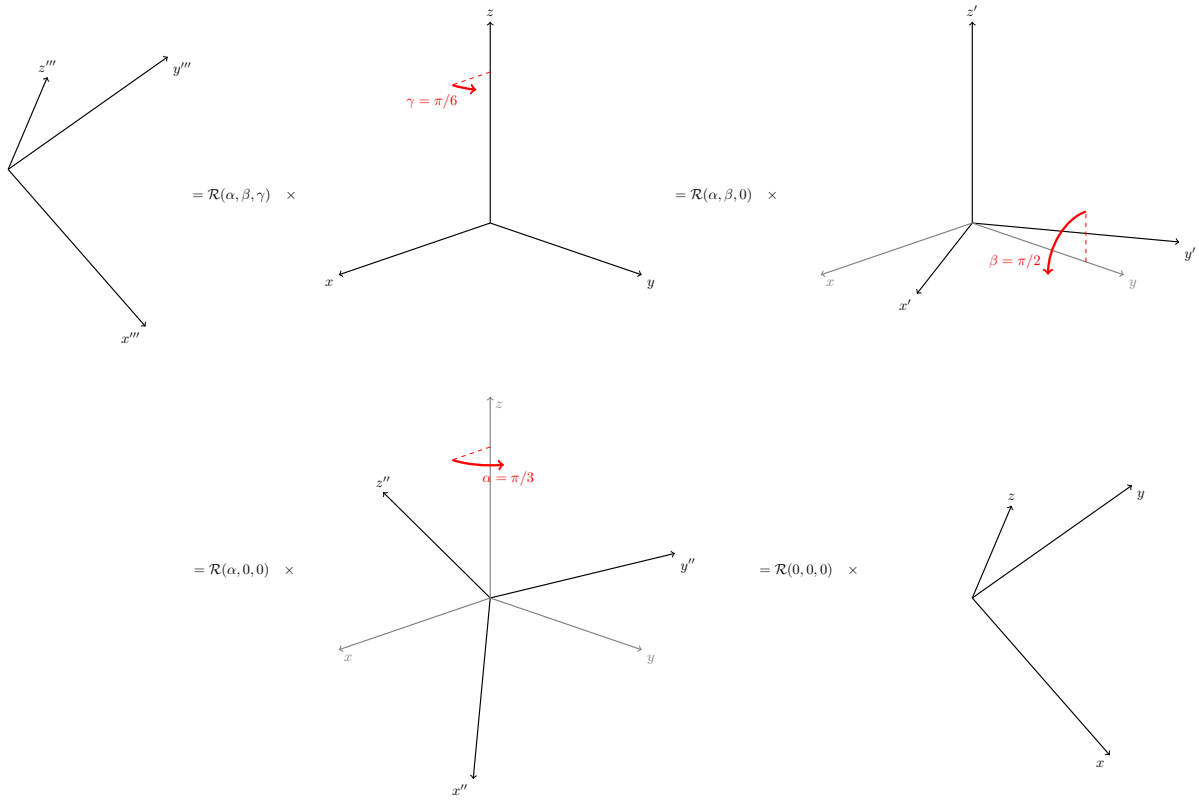

Figure 2.3: Consider a principal axis frame with axes x''', y''' and z'''. Such a PAF frame can be obtained from the lab frame (with axes) x, y and z, by applying three consecutive rotations by angles γ, β, and α about the z, y and z axes respectively.

Table 2.1: g anisotropies for radicals frequently used in EPR. Note that for axially symmetric tensors like trityl, the notation $g_\perp = g_x = g_y$, $g_{||} = g_z$ is often used. Radical data for Tempo from [17], for trityl from [18], for UV radicals from [19]. (Please share a reference for BDPA with me if you have one...)

Radical	g_x	g_y	g_z
Tempo	2.0094	2.0065	2.0017
Trityl (OX063)	2.00319	2.00319	2.00258
BDPA	?	?	?
Keto-UV	2.0036	2.0027	2.0007

To see that this must be so, remember that the tensor rotates and scales the vector. In order to do its job properly on a vector in a different frame, it can rotate this vector back into its own PAF (by applying the inverse rotation R^{-1}), then rotate and scale the vector, and afterwards rotate the resulting vector into the lab frame.

With this rule we can express $\boldsymbol{g}\boldsymbol{S}$ in the lab frame:

$$\boldsymbol{g}\boldsymbol{S}^{[\mathrm{Lab}]} = R\boldsymbol{g}R^{-1}R\boldsymbol{S} = R\boldsymbol{g}\boldsymbol{S} \tag{2.44}$$

$$= \begin{pmatrix} \hat{S}_x g_x \cos(\gamma)\cos(\beta) + \hat{S}_y g_y \sin(\gamma)\cos(\beta) - \hat{S}_z g_z \sin(\beta) \\ -\hat{S}_x g_x \sin(\gamma) + \hat{S}_y g_y \cos(\gamma) \\ \hat{S}_x g_x \sin(\beta)\cos(\gamma) + \hat{S}_y g_y \sin(\gamma)\sin(\beta) + \hat{S}_z g_z \cos(\beta) \end{pmatrix} \tag{2.45}$$

Multiplication by $\boldsymbol{B} = (0, 0, B)$ gives the familiar Hamiltonian with the substitutions $\phi \longrightarrow \gamma$ and $\theta \longrightarrow \beta$.

2.5 Concluding Remarks

We have spent considerable time treating an apparently simple problem - a single electron spin interacting with an external magnetic field. We have seen that the electron Zeeman interaction is markedly different from the nuclear Zeeman interaction. Not only is it larger in size, but it can have an anisotropy of the order of unity. In extreme cases, this implies that the magnetic moment and the spin are not parallel any more.

In addition to the electron Zeeman interaction, many other interactions are important in magnetic resonance. To treat any and all of these, we have to be able to treat spin systems with more than a single spin. This will be the focus of the next lecture.

2.6 Further Reading

- This short lecture can be no substitue for a proper introduction to EPR. An excellent introductory level text by Gunnar Jeschke is available online https://ethz.ch/content/dam/ethz/special-interest/chab/physical-chemistry/epr-dam/documents/education/EPR_PCIV_compressed.pdf .
- For a thorough treatment of EPR have a look at the "folio" by Abragam and Bleaney [14].
- We have only scratched the surface of treating powder averages. For a detailed treatment that takes into account symmetry considerations, have a look at the paper by Brinkmann and Levitt [15].
- To read more about Kernel Density Estimates, and for an excellent text on data analysis at large, have a look at Jahnert's book [16].

2.7 Python

It is useful to easily generate rotation matrices. For example, the code below produces the Euler rotation matrix in the zyz-convention [11]

```
import sympy as sym
from sympy import print_latex

R1 = sym.rot_axis3(sym.Symbol('alpha'))
R2 = sym.rot_axis2(sym.Symbol('beta'))
R3 = sym.rot_axis3(sym.Symbol('gamma'))
R1*R2*R3
```

With the result

$$\mathcal{R}(\alpha,\beta,\gamma)=\begin{pmatrix}-\sin(\alpha)\sin(\gamma)+\cos(\alpha)\cos(\beta)\cos(\gamma) & \sin(\alpha)\cos(\gamma)+\sin(\gamma)\cos(\alpha)\cos(\beta) & -\sin(\beta)\cos(\alpha)\\ -\sin(\alpha)\cos(\beta)\cos(\gamma)-\sin(\gamma)\cos(\alpha) & -\sin(\alpha)\sin(\gamma)\cos(\beta)+\cos(\alpha)\cos(\gamma) & \sin(\alpha)\sin(\beta)\\ \sin(\beta)\cos(\gamma) & \sin(\beta)\sin(\gamma) & \cos(\beta)\end{pmatrix} \tag{2.46}$$

2.8 Exercises

1. Show that the states $\left|\phi_1\right\rangle$ and $\left|\phi_2\right\rangle$ produced by the diagonalization procedure, given by Eq. 2.32 are orthogonal. To do so, calculate $\left\langle\phi_1|\phi_2\right\rangle$ by exploiting the orthonormality of $|\alpha\rangle$ and $|\beta\rangle$. Important: Remember that to obtain the bra to a given ket, you have to conjugate its complex coefficients. That is, if you have a state

$$\left|\phi_1\right\rangle = c_\alpha \left|\alpha\right\rangle + c_\beta \left|\beta\right\rangle ,$$

then the corresponding bra is given by

$$\left\langle\phi_1\right| = c_\alpha^* \left\langle\alpha\right| + c_\beta^* \left\langle\beta\right| .$$

2. Calculate the EPR g spectrum for the Keto-UV radical given in Tab. 2.1. To do so, first define a function in Python that takes two arguments, θ and ϕ, and returns $g_{eff}(\theta, phi)$. You can use the template below to do this. Note the indentation in Python: Everything that is indented by one Tab is part of the function, and the beginning of the function is signalled with the `def` statement. Be sure to take into account that the trigonometric functions are defined for angles in radians, not in degrees.

```
# import numpy module
import numpy as np

def gEff(theta, phi):
    gEff = # your code here
    return gEff
```

Run the function and print the result for a set of values `theta, phi`. Next, define a g-axis using numpys `linspace` command, available as `np.linspace`. Define a Gaussian Function `G(theta, phi, g)` which returns the gaussian Kernel for an orientation defined by `theta, phi` and a list of `g` values. Note that commands like `np.exp` readily calculate the exponentials for all entries in a list as it is produced by `np.linspace` command.
You can plot the Kernel for a particular orientation with this code:

```
import matplotlib.pyplot as plt
plt.plot(gAxis, G(np.pi/2, np.pi/4, gAxis))
plt.show()
```

Note that depending on your setup you may not need the `plt.show()` command.
Finally use the `linspace` command to partition the possible values for ϕ and θ, and use two nested `for` loops to calculate the sum , and plot the result.

3. Give the matrix representation of $\hat{I}_+$ for a spin 3/2 in the Zeeman basis. Can you define a function to give the matrix representation of $\hat{I}_+$ for any integer or half-integer spin?

EPR II. Spin-Spin Interactions | 3

3.1 The Main Ideas

In the previous lecture we have studied the electron Zeeman interaction in detail. Clearly, if we want to understand dynamic nuclear polarization, we need to bring nuclear spins into the picture, and we need to couple the nuclear spins to the electron spins.

In this lecture, we will do precisely that. We will first set out how to describe spin systems with more than one spin. Such a description requires a hilbert space with dimensionality $\Pi_n(2I_n + 1)$, and this is also the dimension of the matrix representation of the respective spin operators. Clearly for systems with more than a handful of spins, the matrices quickly become very large, and more refined techniques have to be used.

However, if we are considering only two or three spins (which is the case here), the matrices are easily dealt with by a computer.

In this lecture, we will use Tempo - the familiar radical form the previous lecture. However, this time, we will also include the hyperfine interaction of the electron spin with the nuclear spin. To treat this system rigorously, we express all the spin operators of the Hamiltonian (which then becomes a 6x6 matrix). We will then find the eigenvalues and eigenvectors of this system using numeric diagonalization.

In this lecture, we will learn

- how to define a basis of spin states for spin systems with more than one spin
- how to diagonalize the hamitonian to find the energy levels of the spin system
- how to use selection rules to calculate the EPR spectrum for Tempo in solids
- how a zero-field-splitting gives rise to a very different energy structure

At the end of this lecture, you will be able to calculate the EPR spectrum of any radical for conditions as they are typical in DNP.

The origin of g-anisotropy

In the last lecture we had a question about the origin of the g-anisotropy. The relevant Hamiltonian to see this effect is given by the sum of the Zeeman interaction and the spin-orbit coupling.

$$\mathcal{H}_Z + \mathcal{H}_{LS} = \mu_B/\hbar \boldsymbol{B}(\boldsymbol{L} + g_e \boldsymbol{S}) + \lambda \boldsymbol{L}\boldsymbol{S}. \tag{3.1}$$

The second term, the spin orbit coupling leads to a little admixture of the higher orbital momentum states into the ground-state. This

causes a shift in energy that depends on the orientation of $\boldsymbol{B}$ and $\boldsymbol{L}$ [20]. But the g-value is simply the derivative of the energy with respect to the field, and so it likewise depends on orientation.

This situation is analogous to Stark shifts which give rise to a molecular polarizability, and which are discussed in some detail by Cohen-Tannoudji [21].

3.2 Hamiltonians with more than one Spin

We want to discuss Hamiltonians for interacting spins, i.e. in particular for Hamiltonians with more than one spin. We will use the nitroxide radical as an example, the procedure is then readily altered or extended to other situations, such as dipolar interacting electron spins.

In the case of nitroxide radicals, the electron spin does not only interact with the magnetic field, but also with the ^{14}N nuclear spin. The interaction is written in general as

$$\mathcal{H} = \frac{\mu_B}{\hbar}\boldsymbol{B}\boldsymbol{g}\boldsymbol{S} + \boldsymbol{S}\boldsymbol{A}\boldsymbol{I} \tag{3.2}$$

Like the g-tensor, the hyperfine tensor has a prinicpal axis frame. In Tempo, the hyperfine tensor is oriented in the same way as the g-tensor, so that we do not have to deal with coordinate transformations. It is given as [17]

$$\boldsymbol{A} = 2\pi \begin{pmatrix} 20.4\,\mathrm{MHz} & 0 & 0 \\ 0 & 17.6\,\mathrm{MHz} & 0 \\ 0 & 0 & 100.8\,\mathrm{MHz} \end{pmatrix} \tag{3.3}$$

For completeness we will later include also the nuclear Zeeman interaction.

We now have to calculate the spectrum of $\mathcal{H}$. This problem may be simplified again, but we rather want to establish a robust method to calculate the spectrum, i.e. one that does not depend on the relative strength of the hyperfine and Zeeman interactions, their relative orientation, etc.

We therefore want to solve the Hamiltonian by direct diagonalization. To do so, we need to express our operators as matrices. We know how to do it for a single spin, but now we have two spins, the electron spin, and the ^{14}N nuclear spin (which is a spin 1).

3.2.1 Two Spin Basis Functions

The elementary basis kets for two spins are the *direct products* of the single spin elmentary basis kets. The possible kets for the electron spin are $|\alpha\rangle$ and $|\beta\rangle$. The kets for the spin 1 are $|1,-1\rangle$, $|1,0\rangle$, $|1,-1\rangle$.

So in total there are now eight basis functions. We have to order them in some way, and we choose to order them first by the electron spin state quantum number m_s and then by the nuclear spin quantum number m_I.

Then the states are

$$|\alpha\rangle \otimes |1,1\rangle = \left|\tfrac{1}{2};1\right\rangle \tag{3.4}$$
$$|\alpha\rangle \otimes |1,0\rangle = \left|\tfrac{1}{2};0\right\rangle \tag{3.5}$$
$$|\alpha\rangle \otimes |1,-1\rangle = \left|\tfrac{1}{2};-1\right\rangle \tag{3.6}$$
$$|\beta\rangle \otimes |1,1\rangle = \left|\tfrac{1}{2};1\right\rangle \tag{3.7}$$
$$|\beta\rangle \otimes |1,0\rangle = \left|\tfrac{1}{2};0\right\rangle \tag{3.8}$$
$$|\beta\rangle \otimes |1,-1\rangle = \left|\tfrac{1}{2};-1\right\rangle \tag{3.9}$$

We have again made use of the short hand notation. We have to keep in mind that the first number in the ket refers to the spin 1/2 electron spin S, and the second number refers to the spin 1 nuclear spin I.

3.2.2 Two Spin Matrix Representations

Now we need to again calculate the matrix representations. The ones for $\hat{I}_z$ and $\hat{S}_z$ are readily written down:

$$\left\langle \hat{I}_z \right\rangle = \begin{pmatrix} 1 & 0 & 0 & 0 & 0 & 0 \\ 0 & 0 & 0 & 0 & 0 & 0 \\ 0 & 0 & -1 & 0 & 0 & 0 \\ 0 & 0 & 0 & 1 & 0 & 0 \\ 0 & 0 & 0 & 0 & 0 & 0 \\ 0 & 0 & 0 & 0 & 0 & -1 \end{pmatrix} \tag{3.10}$$

$$\left\langle \hat{S}_z \right\rangle = \begin{pmatrix} \frac{1}{2} & 0 & 0 & 0 & 0 & 0 \\ 0 & \frac{1}{2} & 0 & 0 & 0 & 0 \\ 0 & 0 & \frac{1}{2} & 0 & 0 & 0 \\ 0 & 0 & 0 & -\frac{1}{2} & 0 & 0 \\ 0 & 0 & 0 & 0 & -\frac{1}{2} & 0 \\ 0 & 0 & 0 & 0 & 0 & -\frac{1}{2} \end{pmatrix} \tag{3.11}$$

The other matrix representations require a bit more work. As an example, we will do $\hat{I}_+$. Remember that $\hat{I}_+$ increases m_I by one. If m_I is already one, the result is zero, so we have to calculate its action on the remaining four basis kets.

$$\hat{I}_+ \left|\tfrac{1}{2};0\right\rangle = \sqrt{1(1+1) - 0(0+1)} \left|\tfrac{1}{2};1\right\rangle = \sqrt{2} \left|\tfrac{1}{2};1\right\rangle \tag{3.12}$$
$$\hat{I}_+ \left|\tfrac{1}{2};-1\right\rangle = \sqrt{1(1+1) - (-1)(-1+1)} \left|\tfrac{1}{2};0\right\rangle = \sqrt{2} \left|\tfrac{1}{2};0\right\rangle \tag{3.13}$$

Note that $\hat{I}_+$ does not act on the spin coordinate of the electron spin, so that one is irrelevant for the calculation:

$$\hat{I}_+ \left|-\tfrac{1}{2};0\right\rangle = \sqrt{1(1+1) - 0(0+1)} \left|-\tfrac{1}{2};1\right\rangle = \sqrt{2} \left|-\tfrac{1}{2};1\right\rangle \tag{3.14}$$
$$\hat{I}_+ \left|-\tfrac{1}{2};-1\right\rangle = \sqrt{1(1+1) - (-1)(-1+1)} \left|-\tfrac{1}{2};0\right\rangle = \sqrt{2} \left|-\tfrac{1}{2};0\right\rangle \tag{3.15}$$

Remember that for matrix representations the row sets the bra, and the column sets the ket. The kets which return a non-zero value when subjected to $\hat{I}_+$ are numbers 2,3,5 and 6 of our basis. So we expect entries in columns 2,3,5, and 6.

They always increase m_I, so the corresponding bras are in rows 1,2, 4 and 5. Thus the first non-zero matrix element is in row 1, column 2, the second in row 2, column 3, and so on. The matrix representation then is

$$\left\langle \hat{I}_+ \right\rangle = \begin{pmatrix} 0 & \sqrt{2} & 0 & 0 & 0 & 0 \\ 0 & 0 & \sqrt{2} & 0 & 0 & 0 \\ 0 & 0 & 0 & 0 & 0 & 0 \\ 0 & 0 & 0 & 0 & \sqrt{2} & 0 \\ 0 & 0 & 0 & 0 & 0 & \sqrt{2} \\ 0 & 0 & 0 & 0 & 0 & 0 \end{pmatrix} \tag{3.16}$$

Now that we understand the mechanics of the spin operators we can of course use a computer to generate the spin operators for us.

Now we can proceed in this way to calculate $\hat{I}_-$, and then again $\hat{I}_x$, and $\hat{I}_y$, and the same for the electron spin operators. Once we have the matrix representations of all the spin operators, we can use them to obtain the matrix representation of the Hamiltonian (the Hamiltonian will again depend on the orientation of the interaction tensors $\boldsymbol{g}$ and $\boldsymbol{A}$ with respect to the applied field *and* with respect to each other). The Hamiltonian matrix is hermitian and in general non-diagonal. To find the energy levels we need to diagonalize it, which - this time - we will actually do numerically only.

Note that the procedure described here is readily extended to spin systems with more than two spins. That said, the matrix dimension for N spins 1/2 is 2^N, and so more elaborate approaches are required once more than a handful of spins are to be simulated.

3.2.3 Diagonalization of the Two Spin Hamiltonian

Let us rewrite the Hamiltonian (3.2) and express all tensors in the lab frame, in which $\boldsymbol{B} = (0, 0, B_0)$. We will use Tempo, and as discussed we have to transform its $\boldsymbol{g}$-tensor into the labframe, using the Euler Rotation Matrix $\mathcal{R}(\alpha, \beta, \gamma)$. The final rotation about the world z-axis is irrelevant, since the external field is applied along the world z-axis. We may therefore set $\alpha = 0$. In general, the hyperfine tensor $\boldsymbol{A}$ may have a PAF that is *rotated* with respect to the $\boldsymbol{g}$-tensor, in which case different Euler angles are required to transform $\boldsymbol{A}$ into the lab frame. In the case of Tempo the $\boldsymbol{g}$-tensor and the hyperfine tensor PAFs have the same orientation.

In such cases, it is a good idea to first transform all interactions into the molecular frame, and then transform them from the molecular frame into the lab frame. This can be done by chaining the rotations. For example, if $\mathcal{R}_1$ transforms the hyperfine tensor into the molecular frame, and $\mathcal{R}_2$ transforms the molecular frame into the lab frame, then $\boldsymbol{A}^{[\mathrm{Lab}]} = \mathcal{R}_2\mathcal{R}_1\boldsymbol{A}^{[\mathrm{PAF}]}\mathcal{R}_1^{-1}\mathcal{R}_2^{-1}$.

We may therefore write the Hamiltonian in the Lab frame as

$$\mathcal{H} = \frac{\mu_B}{\hbar} B_0(0, 0, 1)\mathcal{R}\boldsymbol{g}\mathcal{R}^{-1}\boldsymbol{S} + \boldsymbol{S}\mathcal{R}\boldsymbol{A}\mathcal{R}^{-1}\boldsymbol{I} - \gamma_I B\hat{I}_z \tag{3.17}$$

For a spin system like Tempol, with a spin 1 nucleus and an electron spin 1/2, the matrix representation has dimension 6x6 and is already quite inconvenient to interpret, and a better way to get an idea is to look at a matrix plot.

We can find the proper eigenstates of the Hamiltonian by using the computer to find the eigenvectors of the matrix representation of $\mathcal{H}$.

In the example above, the first basis is the Zeeman product basis, with the states given by Eq. (3.4). For convenience we may write them as $|0\rangle = \left|\frac{1}{2}; 1\right\rangle$, $|1\rangle = \left|\frac{1}{2}; 0\right\rangle$ and so on.

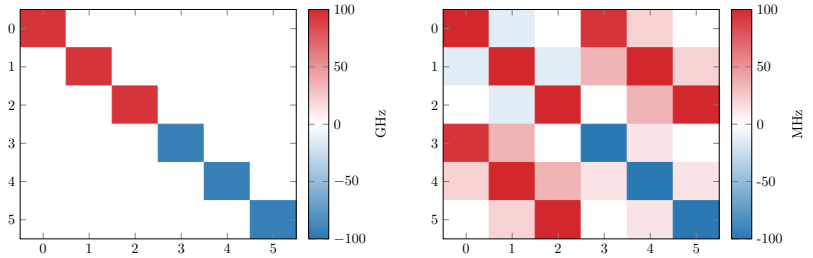

Figure 3.1: Graphical Representation of the real part of the matrix representation of $\mathcal{H}$ in the Zeeman product basis. The Euler angles for $\mathcal{R}$ in (3.17) are $\alpha = 0$, and $\beta = \gamma = 2\pi/3$. The same data as on the left are shown again on the right, but with a different scale. This zoom reveals that the hyperfine term indeed causes the Hamiltonian to be non-diagonal. Note that the plots do not show the complex part of the Hamiltonian.

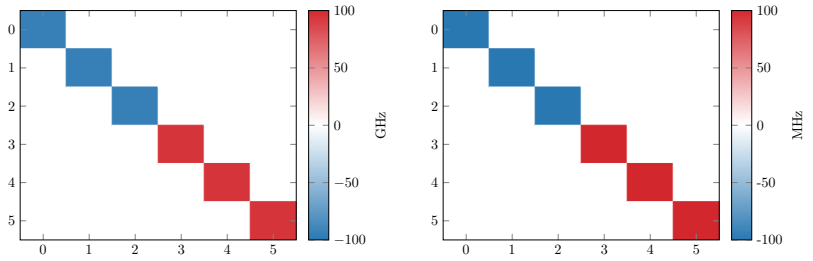

Figure 3.2: The same plot as Fig. 3.1, but now using the Eigenbasis of the Hamiltonian $\mathcal{H}$. The Hamiltonian is now diagonalized, and all non-diagonal elements are zero.

The Eigenvectors happen to be

```
[[ 0.0004+0.j      0.0004+0.j     -0.0001+0.j      0.1314+0.j
   0.478 -0.j     -0.8685+0.j    ]
 [-0.0002+0.0001j  0.0005-0.j     -0.0004+0.j      0.4776-0.0142j
   0.7368-0.0219j  0.4777-0.0142j]
 [ 0.    -0.j     -0.0002+0.0001j -0.0007+0.0001j  0.867 -0.0518j
  -0.4769+0.0284j -0.1313+0.0078j]
 [-0.7392-0.456j  -0.441 -0.1842j  0.125 +0.0403j  0.0002+0.j
   0.0004+0.0001j -0.0003-0.0002j]
 [ 0.414 +0.2387j -0.6884-0.2638j  0.4589+0.1328j  0.0005+0.0001j
   0.0004+0.0002j  0.0002+0.0001j]
 [-0.1158-0.0622j  0.4509+0.1575j  0.8412+0.2166j  0.0007+0.0002j
  -0.0003-0.0001j -0.    -0.j    ]]
```

If we write all eigenvectors in a matrix $\mathcal{M}$, then we can use this matrix to calculate the new eigenstates from the old ones, using

$$|0\rangle' = c' \mathcal{M} |0\rangle , \tag{3.18}$$

where c' ensures normalization. We can do the same for all the other kets. Since $\mathcal{H}$ is hermitian, the eigenvectors are orthogonal, and so the new basis will be ortho-normal.

The matrix representation of the Hamiltonian $\mathcal{H}$ in the new basis (calculated as $\langle 0|' \mathcal{H} |0\rangle'$ and so on, is shown in Fig. 3.2.

The eigenstates in the Hamiltonian are stationary states, but now we need to answer one more question before we can calculate the EPR spectrum. Namely, we need to find out which transitions will be EPR active.

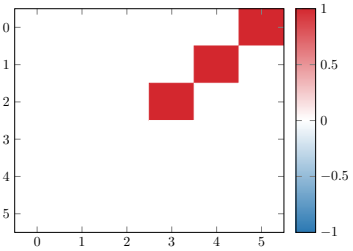

Figure 3.3: Matrix plot of $\left|\langle\phi| S_x |\psi\rangle\right|^2$. The allowed transitions connect the states 0, 1, and 2 with the states 5, 4, and 3, respectively. Note the order of the indices.

3.2.4 Transition Rates

Without an additional interaction, there will be no transitions between the eigenstates of $\mathcal{H}$. The missing bit to induce transitions is a perturbation. In

magnetic resonance this is provided by a radio-frequency or microwave field with a Hamiltonian

$$\mathcal{H}_1 = \frac{mu_B}{\hbar}(B_1, 0, 0)\boldsymbol{g}\boldsymbol{S} \approx \frac{\mu_B}{\hbar} B_1 g \hat{S}_x \tag{3.19}$$

For a discussion of transition rates see [20]. For the case of paramagnetic centres with significant anisotropy, see also [13]

where we have used the fact that for tempo $\boldsymbol{g}$ is nearly isotropic.

Fermi's golden rule states that the transition probability for a transition from an initial state $|0\rangle$ to a final state $|1\rangle$ due to a perturbation $\mathcal{H}_1$ scales as

$$P \sim |\langle 1| \mathcal{H}_1 |0\rangle|^2 . \tag{3.20}$$

We therefore need to calculate the matrix representation of $\mathcal{H}_1$ (or here that of $\hat{S}_x$ *in the rotating frame*) and inspect the square of its absolute values to find out which transitions are allowed [20]. The plot of the squared absolute matrix elements is shown in Fig. 3.3.

It can be seen that the allowed transitions are $|0\rangle \leftrightarrow |5\rangle$, $|1\rangle \leftrightarrow 4$ and $|2\rangle \leftrightarrow |3\rangle$.

3.2.5 EPR Spectrum of TEMPO

Now that we know the energies of the allowed transitions, we can move on and calculate the EPR spectrum. This can be done precisely in the same way as we have done it in the last lecture, but we will now not get one energy (or one Gaussian kernel), but three energies (or three Gaussian kernels) for the three transitions given above. This spectrum is shown as an orange line in Fig 3.4. In general, we may have up to nine transitions (the spin state can change from any of the lower three spin states to any of the higher spin states, and the transition probability is given by the square of the corresponding matrix element).

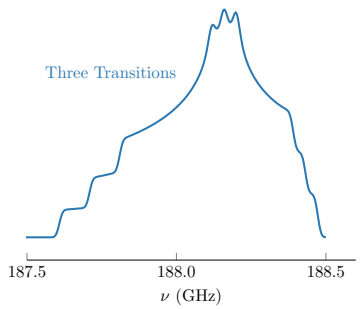

Figure 3.4: EPR spectrum taking into account the three transition rates shown in Fig. 3.3

We finish this lecture with a discussion of the dipolar interaction of two electron spins, and the zero-field interaction, which - in analogy to the nuclear quadrupole interaction - is modelled as an interaction of the electron spin with itself.

3.3 Dipolar Interaction

In the same way that we have specified the hyperfine interaction, we can specify all the other interactions. The dipolar interaction of two electron spins $\boldsymbol{S}_1$ and $\boldsymbol{S}_2$ may be written, in general as

$$\mathcal{H}_{DD} = \boldsymbol{S}_1 \boldsymbol{D} \boldsymbol{S}_2, \tag{3.21}$$

where $\boldsymbol{D}$ is the dipole-dipole coupling tensor. Neglecting g-anisotropy, we assume the g-factors of spins 1 and 2 to be given by g_1 and g_2. Then we may write the dipolar hamiltonian as

$$\mathcal{H}_{DD} = \boldsymbol{S}_1 \boldsymbol{D} \boldsymbol{S}_2 = \frac{\mu_0}{4\pi\hbar} \frac{g_1 g_2 \mu_B^2}{r_{12}^3} \left[\boldsymbol{S}_1 \boldsymbol{S}_2 - \frac{3}{r_{12}^2} (\boldsymbol{S}_1 \boldsymbol{r}_{12})(\boldsymbol{S}_2 \boldsymbol{r}_{12}) \right] \tag{3.22}$$

In its principal axis frame, the dipole-dipole tensor may be written as

$$\boldsymbol{D}^{[\mathrm{PAF}]} = \frac{\mu_0}{4\pi\hbar}\frac{g_1 g_2 \mu_B^2}{r_{12}^3}\begin{pmatrix} -1 & 0 & 0 \\ 0 & -1 & 0 \\ 0 & 0 & 2 \end{pmatrix} \tag{3.23}$$

The dipolar Hamiltonian may also be expressed using the dipolar alphabet [6] (where θ is the angle between the vector $\boldsymbol{r}$ that connects the two spins, and the applied magnetic field):

$$\mathscr{H}_{DD} = \frac{g_1 g_2 \mu_B^2}{r^3}\frac{\mu_0}{4\pi\hbar}\left[\hat{A} + \hat{B} + \hat{C} + \hat{D} + \hat{E} + \hat{F}\right], \tag{3.24}$$

where

$$\hat{A} = \hat{S}_{1z}\hat{S}_{2z}(1 - 3\cos^2\theta) \tag{3.25}$$

$$\hat{B} = -\frac{1}{4}\left(\hat{S}_{1+}\hat{S}_{2-} + \hat{S}_{1-}\hat{S}_{2+}\right)(1 - 3\cos^2\theta) \tag{3.26}$$

$$\hat{C} = -\frac{3}{2}\left(\hat{S}_{1+}\hat{S}_{2z} + \hat{S}_{1z}\hat{S}_{2+}\right)\sin\theta cos\theta\exp(-\mathrm{i}\phi) \tag{3.27}$$

$$\hat{D} = -\frac{3}{2}\left(\hat{S}_{1-}\hat{S}_{2z} + \hat{S}_{1z}\hat{S}_{2-}\right)\sin\theta\cos\theta\exp(\mathrm{i}\phi) \tag{3.28}$$

$$\hat{E} = -\frac{3}{4}\hat{S}_{1+}\hat{S}_{2+}\sin^2\theta\exp(-2\mathrm{i}\phi) \tag{3.29}$$

$$\hat{F} = -\frac{3}{4}\hat{S}_{1-}\hat{S}_{2-}\sin^2\theta\exp(2\mathrm{i}\phi) \tag{3.30}$$

Now, if we assume that the spins are quantized along the external magnetic field (the high-field approximation), we see that (i.e. one that is significantly larger than the dipolar interaction), the eigen-states we see that the term $\hat{B}$ corresponds to a flip-flop processes. Such flip-flop processes are required for spin diffusion, an important mechanism to spread nuclear polarization across the sample.

The terms $\hat{C}$ to $\hat{F}$ on the other hand involve a change of energy. Consequentially, these terms may often be discarded.

3.4 Zero-Field-Splitting

We now discuss the zero-field splitting. This term plays a role for spins > 1/2, and is analogous to the nuclear quadrupole interaction. A prominent system exhibiting a significant zero-field-splitting is molecular oxygen, which is modelled as an electron spin 1 with $g \approx 2$. We will keep with the literature convention and use the symbol $\boldsymbol{D}$ also for the zero-field-splitting.

The Zero-Field-Splitting Hamiltonian is written as

$$\mathscr{H}_{ZFS} = \boldsymbol{SDS}. \tag{3.31}$$

The Hamiltonian may be written in the PAF Frame as

$$\mathcal{H}_{ZFS}^{[\mathrm{PAF}]} = \boldsymbol{SDS} = \hat{S}_x^2 D_x + \hat{S}_y^2 D_y + \hat{S}_z^2 D_z \tag{3.32}$$

$$= D\left[\hat{S}_z^2 - \frac{1}{3}\mathbf{1}S(S+1)\right] + E(\hat{S}_x^2 - \hat{S}_y^2), \tag{3.33}$$

with $D = 3D_z/2$ and $E = (D_x - D_y)/2$.

We may write the Zeeman Hamiltoninan in the PAF of the zero-field-splitting using the directional cosines l, m, n. For oxygen, we have $S = 1$, $E = 0$, and $D \approx 95$ GHz [22]. Then, the total Hamiltonian is

$$\mathcal{H} = \mathcal{H}_Z + \mathcal{H}_{ZFS} = \frac{\mu_B}{\hbar} gB(l\hat{S}_x + m\hat{S}_y + n\hat{S}_z) + D\left[\hat{S}_z^2 - \frac{2}{3}\mathbf{1}\right] \tag{3.34}$$

The Eigenvalues of this Hamiltonian are shown in Fig.. The significane of the large zero-field-splitting is that it allows oxygen to couple to phonons even at very low field. In doing so, it attains fast relaxation, and may likewise relax other paramagnetic species as well as nuclei.

3.5 Concluding Remarks

In this lecture we have introduced spin states for spin systems with more than one spin, and how to diagonalize the respective Hamiltonians. We have seen relevant spin interactions for DNP, and we have seen how these can be used to calculate the EPR spectrum.

We have also seen that the different spin terms in the Hamiltonian may be interpreted as causing transitions between levels, such as the flip-flops of two interacting electron spins.

In the next lecture, we will see how a perturbation such as a microwave source can cause double flips of electron and nuclear spins (the solid and Overhauser effect), and we will also see triple-spin-flip.

3.6 Further Reading

[23]: Wenckebach (2016), *Essentials of Dynamic Nuclear Polarization*

- For an alternative way of arriving at the TEMPO EPR spectrum, have a look at Wenckebach's Essentials of Dynamic Nuclear Polarization [23]. Wenckebach's text on the whole is an inspiring demonstration of how the right approximations can shed light onto a complex problem (which dynamic nuclear polarization undoubtedly is).
- Not exactly further reading, but it may pay to explore other software packages for spin dynamical simulations. Apart from SpinDynamica (which is written in Mathematica) there are the Matlab written EasySpin for EPR simulations, and of course Spinach. EasySpin is comparatively lightweight and does not need any additional Toolboxes, but Spinach arguably has a broader scope.
- An inferior, but easily available home-written software to express spin operators in Python is Spinthon. Spinthon uses oject-oriented programming to define entities like kets and spin operators, and operator overloading to define multiplications of these entities.

Spinthon is available on PyPi. For details on the underlying programming techniques have a look at Ramalho's Fluent Python [24].

[24]: Ramalho (2015), *Fluent Python*

3.7 Python

```
# to get the eigenvalues of a matrix m
import numpy as np

M = np.array([..])

eigvecs, eigvals = np.linalg.eig(M)

# if M is hermitian, we can use
eigvecs, eigvals = np.linalg.eigh(M)
```

In order to use `spinthon` for the exercises, you have to install it. To do so, on a terminal type

```
pip install spinthon
```

3.8 Exercises

1. Diagonalize the Hamiltonian for oxygen, with the parameters given in the lecture notes, for a set magnetic field strength, and for an orientation defined by the orientational cosines l, m, n.
   First obtain the spin operators using the software package of your choice. In `spinthon` you can pretend that you want to study a ^{14}N nucleus. You can get the spin operator as follows:

   ```
   import numpy as np
   import spinthon

   from spinthon.spin.operators import SpinOperator,
     VectorSpinOperator
   from spinthon.spin.system import SpinSystem

   S1 = SpinSystem(["14N"])

   Sx = SpinOperator(S1, 0, "Ix")
   SxM = Sx.getMatrixRepresentation()
   ```

   To get the y and z operators simply replace `Ix` with `Iy` etc. For setting up the Hamiltonian you also need a unity matrix. This can be created with the `np.diag` command. Once you have the matrix you can try to visualize its real and imaginary parts using the `matplotlib` command `matshow`. Can you find a suitable colour scale? Can you guess what happens to the matrix when you set $m = 1$ and $l = n = 0$?
   For $m = 1$, $l = n = 0$, check that the matrix of eigenvectors $\boldsymbol{M}$ diagonalizes the Hamiltonian by exectuing the multiplication $\boldsymbol{MHM}^{-1}$, where $\boldsymbol{H}$ is the matrix representation of the Hamiltonian as calculated with the spin operators obtained from `spinthon`.

2. In a next step use the code from Ex. 1 and write a function that returns the oxygen energy levels for a given field and orientation, where the orientation is specified by the angles ϕ and θ.
3. If you feel a little bit more comfortable with Python, and are willing to do some online searching, have a go at object oriented programming with Python. Define a `Counter` class with an `__init__` method that sets an internal counter to an initial value which is passed to the init method. The class should also define methods `plusOne` and `minusOne` that increment or decrement the counter value, as well as methods `plusAny` and `minusAny` that allow you to add or subtract an arbitrary integer to the counter value. Note that such a class has little use in and of its own, but that the example is a step towards defining classes that are actually useful for dealing with spin Hamiltonians. A template for such a class is given below.

```
class Counter(object):
    def __init__(self, initialValue):
        # yourCodehere

    def plusOne(self):
        # yourCodehere

    def minusOne(self):
        # yourCodehere

    def plusAny(self, value):
        # yourCodehere

    def minusAny(self, value):
        # yourCodehere
```

DNP I. Electron-Nuclear Polarization Transfer

4

4.1 The Main Ideas

In the previous lecture we have studied spin interactions in detail. We have learned that the electron Zeeman interaction is much larger than the nuclear Zeeman interaction, and we have seen how nuclear and electron spins are coupled by hyperfine interactions.

In this lecture we will see how the hyperfine coupling may be used to transfer large electron spin polarization to the hyperfine coupled nucleus. This process may unfold in different ways.

In the solid effect, we make use of a forbidden transition, and use a microwave to drive this transition, an electron flip-flop. In doing so, we force the populations of the two involved states to become equal, and consequentially we end up with a high polarization.

In the Overhauser effect (which historically was discovered before the solid effect), we saturate a pure electron transition, but exploit relaxation to end up with high nuclear polarization.

In thermal mixing, or the cross effect, we use triple-spin-flips involving *two* electron spins and one nuclear spin. Here, the energy that is released (or absorbed) by an electron-electron flip-flop has to be matched by the absorbed (or released) energy of the nuclear spin transition. In the limit of high electron spin polarization, we can for example saturate one electron transition, such that then electron-electron flip-flops only release energy. This means that the ensuing triple-spin-flip must cause the nucleus to absorb energy, and so the population of the nuclear Zeeman state with higher energy increases.

In this lecture, we will learn

- how the same energy structure underpins the solid effect and the Overhauser effect
- how rate equations can be used to calculate the final polarization of the nuclear spin
- how the solid effect and the Overhauser effect become weaker as the magnetic field is increased
- how triple spin flips can be used for DNP when the solid effect doesn't work anymore
- how a DNP spectrum gives information on the DNP mechanisms at play

At the end of this lecture, you will know which DNP mechanism is important at a given field. Note that we will defer any considerations of bulk effects, nuclear spin diffusion, etc. to the next lecture.

4.2 The Solid- and the Overhauser Effect

4.2.1 Energy Structure

The key ingredients of both the Solid- and the Overhauser-Effect are the electron and nuclear Zeeman interaction, and a hyperfine coupling. We have discussed these interactions in detail in the previous lectures. Here, we will use a very simple model to illustrate how these interactions can give rise to sizeable nuclear spin polarization.

We assume a purely isotropic electron Zeeman interaction, and write the Hamiltonian as

$$\mathcal{H} = \frac{\mu_B g B}{\hbar}\hat{S}_z + \boldsymbol{SAI} - \gamma_I B\hat{I}_z \tag{4.1}$$

The largest interaction in this Hamiltonian is the electron Zeeman interaction, and, consequentially m_S is a good quantum number. In general, we can find the eigenstates for $\mathcal{H}$ using the numeric procedures outlined in the previous lecture.

Now we assume that we have a nuclear spin 1/2, and we furthermore assume that the nuclear Zeeman interaction is *larger* than the hyperfine interaction.[1] In this case, also m_I is a good quantum number, and the Hamiltonian may be written as

$$\mathcal{H} = \frac{\mu_B g B}{\hbar}\hat{S}_z + A\hat{S}_z\hat{I}_z - \gamma_I B\hat{I}_z \tag{4.2}$$

The energy levels are given by

$$E = \frac{\mu_B g B}{\hbar}m_S + Am_S m_I - \gamma_I B m_I. \tag{4.3}$$

These states are shown in Fig. 4.3. Note that the hyperfine interaction splits both the NMR and the EPR transition into two lines, and that the splittings are not drawn to scale.

The energy structure can be used to understand both the Overhauser effect and the solid effect. In the Overhauser effect, one irradiates at a frequency corresponding to one of the EPR transitions, and relies on cross-relaxation to generate nuclear spin polarization. In the solid effect, one applies a microwave irradiation accross a so called forbidden transition, i.e. one drives an electron-nuclear flip-flip, or flip-flop. We will now look at these two effects in much greater detail. The treatment closely follows Slichter's chapter on double resonance [6].

4.2.2 The Overhauser Effect

We know from the first lecture, that in thermal equilibrium we can calculate the thermal equilibrium populations of the four energy levels using the Boltzmann distribution. We also know that following a perturbation the system will reach thermal equilibrium again, via transitions between the energy levels. We can of course actively drive transitions by applying a microwave field with a resonance frequency that is matched to one of the EPR transitions. The transition rate W_e of this driven transition

1: This assumption will apply for nuclei which are further away from the radical (for instance when we use a large radical like trityl), and at high field. It does *not* apply for nuclei close to the radical and at low field.

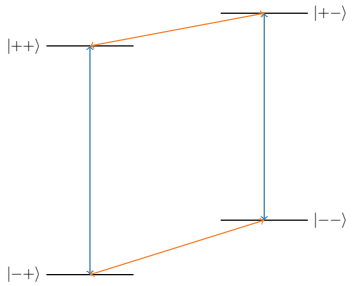

Figure 4.1: Energy levels of an electron spin and a nuclear spin which are coupled by a hyperfine coupling. In NMR on observes nuclear spin flips (orange transitions), in EPR one observes electron spin flips (blue transitions). Note that the hyperfine interaction splits both the electron spin and the nuclear spin resonance. The electorn Zeeman interaction is orders of magnitude larger than the other interactions - the drawing is not to scale, but rather uses the ratio E/N/A = 5/1/0.5 for the electron, nuclear and hyperfine terms.

[6]: Slichter (1990), 'Principles of Magnetic Resonance'

will depend on the strength of the microwave field. For high microwave fields, the transition will get saturated, which is the same as saying that the populations of the two involved levels will equilibrate.

The dynamics are described by a set of four differential equations for the four energy levels:

$$\frac{dp_1}{dt} = p_2 W_{21} - p_1 W_{12} + p_4 W_{41} - p_1 W_{14} + (p_2 - p_1) W_e \tag{4.4}$$

$$\frac{dp_2}{dt} = -p_2 W_{21} + p_1 W_{12} - (p_2 - p_1) W_e \tag{4.5}$$

$$\frac{dp_3}{dt} = p_4 W_{43} - p_3 W_{34} \tag{4.6}$$

$$\frac{dp_4}{dt} = p_1 W_{14} + p_3 W_{34} - p_4 W_{43} - p_4 W_{41} \tag{4.7}$$

Once we achieve equilibrium, the transitions do no longer lead to changes in the net population of the respective levels, and

$$\frac{dp_i}{dt} = 0. \tag{4.8}$$

The probabilities of being in any particular state have to add to 1:

$$p_1 + p_2 + p_3 + p_4 = 1 \tag{4.9}$$

If W_e is sufficiently strong, we will achieve saturation accross the transition $|1\rangle \leftrightarrow |2\rangle$, and hence

$$p_1 = p_2 \tag{4.10}$$

From Eq. 4.6, we have

$$p_3 = p_4 \frac{W_{43}}{W_{34}}, \tag{4.11}$$

and from Eqs. (4.6) and (4.7) we have

$$p_1 = p_4 \frac{W_{41}}{W_{14}} \tag{4.12}$$

The transition $|3\rangle \leftrightarrow |4\rangle$ is in thermal equilibrium, as is the transition $|1\rangle \leftrightarrow |4\rangle$. The population ratio accross these transitions is hence given by the Boltzmann distribution

$$\frac{p_i}{p_j} = \exp\left(-\left(E_i - E_j\right)/kT\right) \tag{4.13}$$

This may be rewritten as

$$\underbrace{p_i \exp\left(+\left(E_i - E_j\right)/kT\right)}_{B_{ij}} = p_j \tag{4.14}$$

where we have introduced the symbol B_{ij} with

$$p_i B_{ij} = p_j \tag{4.15}$$

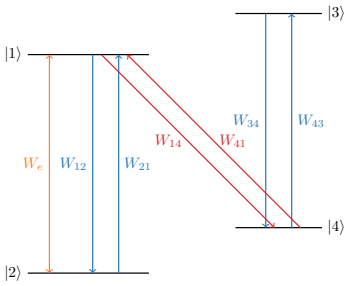

Figure 4.2: The same drawing as 4.3, but this time with the scaling E/N/A = 5/1/0.1. The state label has been changed to simplifiy the notation, according to $|1\rangle = |{+}{+}\rangle$, ... Instead of the NMR and EPR transitions, the EPR transition rates are shown, as well as the transition rates of electron-nuclear flip-flops as they arise due to the Fermi contact interaction.

and with

$$B_{ij} = 1/B_{ji} \tag{4.16}$$

and

$$\frac{B_{ix}}{B_{kx}} = B_{ik} \tag{4.17}$$

We rewrite Equations (4.11) and (4.12) as

$$p_3 B_{34} = p_4 \tag{4.18}$$

and

$$p_1 B_{14} = p_4 \tag{4.19}$$

Now we use these two expressions to eliminate p_4, and we eliminate p_2 by inserting $p_1 = p_2$ into Eq. (4.9), and we have

$$p_3 B_{34} = p_1 B_{14} \tag{4.20}$$

$$2p_1 + p_3 + p_3 B_{34} = 1 \tag{4.21}$$

We use the first equation to eliminate p_3 in the second, and obtain

$$2p_1 + p_1 \frac{B_{14}}{B_{34}} + p_1 B_{14} = 1, \tag{4.22}$$

and hence

$$p_1 = p_2 = \frac{1}{2 + \frac{B_{14}}{B_{34}} + B_{14}} = \frac{1}{2 + B_{13} + B_{14}} \tag{4.23}$$

We furthermore have

$$p_4 = p_1 B_{14} = \frac{B_{14}}{2 + B_{13} + B_{14}} \tag{4.24}$$

and

$$p_3 = p_4 / B_{34} = \frac{B_{13}}{2 + B_{13} + B_{14}} \tag{4.25}$$

Now let us see whether these populations give rise to stronger NMR signals. To do so, we need to calculate the expecation value of $\hat{I}_z$. To do so, we need to calculate the expectation value of $\hat{I}_z$ in all populated levels, multiply each value with the respective populations, and calculate the sum. The result is

$$\left\langle \hat{I}_z \right\rangle = p_1 \langle 1| \hat{I}_z |1\rangle + p_2 \langle 2| \hat{I}_z |2\rangle \tag{4.26}$$

$$+ p_3 \langle 3| \hat{I}_z |3\rangle + p_4 \langle 4| \hat{I}_z |4\rangle \tag{4.27}$$

$$= \frac{1}{2} (p_1 + p_2 - p_3 - p_4) \tag{4.28}$$

$$= \frac{1}{2} \left(\frac{2 - B_{13} - B_{14}}{2 + B_{13} + B_{14}} \right) \tag{4.29}$$

Now we insert the high-temperature approximation $B_{ij} \approx 1 + \frac{(E_i - E_j)}{kT}$, etc.

Then we have

$$\left\langle \hat{I}_z \right\rangle = \frac{1}{2} \frac{2 - \left(1 + \frac{E_1 - E_3}{kT}\right) - \left(1 + \frac{E_1 - E_4}{kT}\right)}{4} \tag{4.30}$$

$$= -\frac{1}{2} \frac{(E_1 - E_3) + (E_1 - E_4)}{4kT} \tag{4.31}$$

$$= -\frac{1}{2} \frac{2E_1 - E_3 - E_4}{4kT} \tag{4.32}$$

The dominant electron Zeeman energy is $E_1 \sim \frac{1}{2}\gamma_e B$ in level, where as the same terms $-\frac{1}{2}\gamma_e B$ cancel each other in levels 3 and 4. As usual, $\gamma_e = \mu_B g/\hbar$ is the gyromagnetic ratio of the free electron spin. Then we have

$$\left\langle \hat{I}_z \right\rangle = -\frac{1}{2} \frac{\hbar \gamma_e B}{4kT} \tag{4.33}$$

On the other hand, from the first lecture, we have for nuclear spins at thermal equilibrium

$$\left\langle \hat{I}_z \right\rangle_{\text{therm. eq.}} = IP = \frac{1}{2} \frac{\hbar \gamma_I B}{2kT} \tag{4.34}$$

The ratio of these two is

$$\left| \frac{\left\langle \hat{I}_z \right\rangle}{\left\langle \hat{I}_z \right\rangle_{\text{therm. eq.}}} \right| = \frac{\gamma_e}{2\gamma_I} \tag{4.35}$$

If one saturates both transitions, the factor two disappears, and the enhancement is

$$\left| \frac{\left\langle \hat{I}_z \right\rangle}{\left\langle \hat{I}_z \right\rangle_{\text{therm. eq.}}} \right| = \frac{\gamma_e}{\gamma_I} \tag{4.36}$$

which corresponds to ≈ 660 for protons, and is even larger for nuclei with a lower gyromagnetic ratio.

The Nuclear Overhauser Effect

While Overhauser made his prediction for nuclear spins in metals, his formalism is by no means limited to this material. Today, Overhauser DNP is typically carried out using solutions containing radicals. The process works best at high fields, although - depending on the mechanism that drives the electron-nuclear relaxation, it may also be carried out at higher field [25].

The principle established by Overhauser may also be applied to coupled nuclear spins. Changing the polarization accross a transition of one of the spins leads to detectable changes in the polarization of coupled spins via homo- or hetero-nuclear cross-relaxation. This nuclear overhauser effect (NOE) gives indispensable information about the coupling, and hence the structure of nuclear spin networks.

[25]: Ravera et al. (2016), 'Basic Facts and Perspectives of Overhauser DNP NMR'

4.2.3 The Solid Effect

In insulating solids, a rapid electron-nuclear relaxation process W_{14} is often not available. It turns out that there still is a way to polarize nuclear spins. In our simplified treatment of the Hamiltonian (4.1), the Zeeman states were the eigenstates of both the electron and the nuclear spins. This solution becomes increasingly accurate, as the nuclear Zeeman interaction dominates the hyperfine interaction.

An exact solution of ((4.1) however leads to eigenstates, in which the nuclear spin part is a mixture of nuclear Zeeman states. The quantum number m_S then is still a good quantum number, but m_I is not. Instead, the eigenstates are linear combinations of the Zeeman product states:

$$|1\rangle' = c_1 \left|\frac{1}{2}\right\rangle \otimes \left|\frac{1}{2}\right\rangle + c_2 \left|\frac{1}{2}\right\rangle \otimes \left|-\frac{1}{2}\right\rangle \tag{4.37}$$

As was realized by Jeffries [26] and independently by Abragam, the admixture of "a little bit of $\left|-\frac{1}{2}\right\rangle$" into the state $|1\rangle$ creates a finite transition element between the states $|1\rangle$ and $|4\rangle$, if a microwave field is applied that oscillates at the energy difference of states $|1\rangle$ and $|4\rangle$.

The same is true for the states $|2\rangle$ and $|3\rangle$, although here a higher microwave frequency is required. Now if we consider the case where the hyperfine interaction is sufficiently large to allow such transitions, but otherwise small compared to the Nuclear Zeeman interaction, we find that we can create positive and negative polarization if we drive transitions at a frequency $\omega_S - \omega_I$ and $\omega_S + \omega_I$ respectively.

In DNP experiments, one typically records the NMR signal as a function of the microwave frequency. The plot of intensity vs. frequency is called a DNP spectrum. A clear solid effect is observed when (i) the employed radical is a narrow-band radical and (ii) when the DNP process is carried out at a relatively low field. As an example, a clear solid effect is obtained for trityl and ^{13}C polarization at 3.35 Tesla. Under the same conditions, no solid effect is obtained for protons, because the transition matrix element for protons is too small for typical microwave sources.

For DNP experiments at 6.7 T and higher, the solid effect is not typically observed. This may however change, when one replaces todays solid-state microwave sources e.g. with klystrons or gyrotrons.

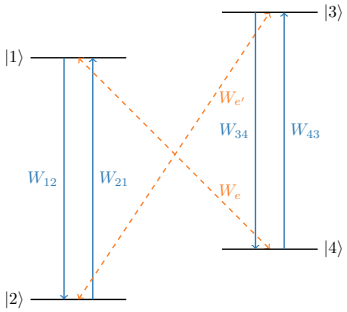

Figure 4.3: The same diagram as 4.2. In the solid effect, a relaxation mechanism for transitions such as $|1\rangle \leftrightarrow |4\rangle$ is absent. However, the transition may be driven by microwave irradiation. Depending on the frequency of the microwave irradiation either positive W_e or negative nuclear spin polarizatoin W_e' is obtained.

[26]: Jeffries (1957), 'Polarization of Nuclei By Resonance Saturation in Paramagnetic Crystals'

Insert DNP Spectrum

4.3 Triple-Spin-Flip DNP

We now turn to an important class of DNP mechanisms, in which not one, but two electrons are used to polarize a coupled nuclear spin. The idea in triple spin flips is that we apply a magnetic field and low temperatures, to establish a highly polarized electron spin system. We can then use a microwave source to saturate a subset of the eletron spins. If we apply the microwave irradiation at a suitable frequency, triple-spin-flips (TSFs) comprising an electron-electron flip-flop and a nuclear spin flip lead to a substantial nuclear spin polarization. In these triple spin flip energy is exchanged between the two electron spins on the one hand, and the nuclear spin on the other hand. The triple-spin flip conserves energy,

and hence the change in nuclear Zeeman is matched by a corresponding change in electron energy.

The Hamiltonian may be written in general by considering two electrons i and j, coupled to each other with a dipolar coupling $\boldsymbol{D}$, and with one of them coupled to a nucleaer spin via a hyperfince coupling $\boldsymbol{A}$.

$$\mathscr{H} = \omega_i \hat{S}_z^i + \omega_j \hat{S}_z^j - \omega_I \hat{I}_z + \boldsymbol{S}^i \boldsymbol{A} \boldsymbol{I} + \boldsymbol{S}^i \boldsymbol{D} \boldsymbol{S}^j \tag{4.38}$$

If the g-anisotropy of the radical is sufficiently large (such that the the electron Larmor frequencies of two suitable nuclear spins ω_j and ω_i differ by the nuclear Larmor frequency ω_I), then the entire nuclear Zeeman energy may be absorbed (or released) in (or from) electron Zeeman energy. In this process, shown in Fig. 4.4, the electron-electron dipolar interaction and the electron-nuclear hyperfine interaction merely serve to mediate the exchange of Zeeman energy.

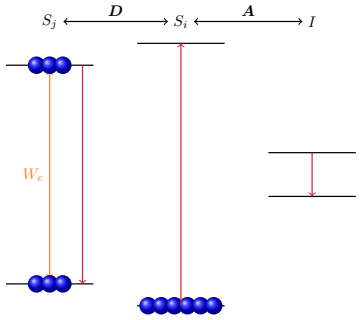

Figure 4.4: The Cross Effect. The Larmor frequency of two electron spins differs by the nuclear Larmor frequency. The populations of the electron spins are shown after the microwave (W_e) has saturated the transition at lower frequency. Then, triple-spin-flips can occur in which S_j flips, to the lower energy level, S_i flops to the upper level, and the required excess energy is released by a nuclear spin flip. As a result the popuplation of the lower nuclear spin level increases.

The nuclear Zeeman energy may be absorded (or released) in (or from) other terms in the electron spin Hamiltonian. In this case, we use the term electron non-Zeeman energy. In a radical like trityl, this contribution is dominated by electron dipole-dipole interactions. In nitroxide radicals, the hyperfine interaction may contribute, and so one then uses the term Non-Zeeman energy for all the energies *except* for the electron Zeeman energy.

Of course, a triple-spin-flip may exchange nuclear Zeeman energy with both electron Zeeman energy *and* electron Non-Zeeman energy.

To see how these effects can come about, we follow [23] and first rewrite the Hamiltonian (4.38) using step operators. The result is

$$\begin{aligned}\mathscr{H} =& \omega_i \hat{S}_z^i + \omega_j \hat{S}_z^j - \omega_I \hat{I}_z \\ &+ A_{zz} \hat{S}_z^i \hat{I}_z + \frac{1}{2} A_{z-} (\hat{S}_z^i \hat{I}_+ + \hat{S}_+^i \hat{I}_z) + \frac{1}{2} A_{z+} (\hat{S}_z^i \hat{I}_- + \hat{S}_-^i \hat{I}_z) \\ &+ D_{zz} \hat{S}_z^i \hat{S}_z^j + \frac{1}{2} D_{z-} (\hat{S}_z^i \hat{S}_+^j + \hat{S}_+^i \hat{S}_z^j) + \frac{1}{2} D_{z+} (\hat{S}_z^i \hat{S}_-^j + \hat{S}_-^i \hat{S}_z^j)\end{aligned} \tag{4.39}$$

where $A_{z+} = A_{zx} + \mathrm{i} A_{zy}$, and $A_{z-} = A_{zx} - \mathrm{i} A_{zy}$, and we have made use of the symmetry of $\boldsymbol{A}$.

Now we separate this Hamiltonian into a diagonal Hamiltonian, and a non-diagonal Hamiltonian. The non-diagonal part will then drive transitions between the states of the diagonal Hamiltonian.

[...]

As we have seen in the first lecture, a change in nuclear polarization corresponds to a change in *spin temperature*. At this point, a comment on nomenclature is due. The process, in which electron Zeeman energy is exchanged with nuclear Zeeman energy is universally referred to as the *cross-effect*.[2] The process in which electron non-Zeeman energy is exchanged with nuclear Zeeman energy is termed *thermal mixing*. Frequently the term thermal mixing is used for the family of DNP processes that involve triple-spin-flips. Here, to avoid ambiguity, we use the term *triple-spin-flip DNP* for this family, and the terms *cross-effect DNP* and *thermal mixing DNP* for its members.

[23]: Wenckebach (2016), *Essentials of Dynamic Nuclear Polarization*

2: In MAS-DNP one uses biradicals with g-values engineered in such a way that the difference in electron Larmor frequencies is close to the nuclear Larmor frequency.

4.4 Concluding Remarks

In this chapter we have seen a range of DNP experiments, which have been observed under very different experimental conditions. What all of these have in common is that microwave irradiation is used to create a non-equilibrium electron polarization. In the case of the Overhauser effect this non-equilibrium electron polarization leads to nuclear polarization via cross-relaxation. In the case of the solid-effect, the non-equilibrium nuclear polarization is created directly, since the microwave transition drives an electron-nuclear flip-flop. Finally, in triple-spin-flip DNP, the microwave is used to create an electron spin polarization such that triple-spin-flips are possible that either preferrably flip, or preferrably flop a nuclear spin.

In this chapter, we have treated these effects for very simple spin systems, consisting of only four spins. To model the dynamics of real-world systems, in which many spins interact, we will need the concept of spin temperature, which is the topic of the next lecture.

4.5 Further Reading

- Although DNP experiments are technically challenging even today, they are among the first double-resonance experiments that have ever been carried out. Chapter 7 of Slichter's Principles of Magnetic Resonance is a very elegant exposition of the basic physics of such experiments.
- A thorough treatment of the solid effect and triple-spin-flip DNP, has been given by Wenckebach's *Essenstials of Dynamic Nuclear Polarization* [23]. Two more recent papers of his introduce the nomenclature that we also employ in this lecture [27, 28].

4.6 Python

The code below shows one way of implementing the differential equations for the Overhauser Effect in Python.

```
# energies of states E1 = ++ and E2 = -+
gE = spindata.gamma("E")
gN = spindata.gamma("1H")
B = 5
T = 100

# calculate the populations of the levels in thermal equilibrium
# taking into account both the electron and the nuclear Zeeman
    interaction
E1 = hbar*(1/2*gE*B-1/2*gN*B)
E2 = -hbar*(1/2*gE*B  + 1/2*gN*B)
E3 = hbar*(1/2*gE*B + 1/2*gN*B)
E4 = hbar*(-1/2*gE*B + 1/2*gN*B)

B12 = np.exp((E1 - E2)/(k*T))
B34 = B12
B14 = B12
```

```
print(E1)
print(E2)
print(E3)
print(E4)

# calculate the partition sum (this is 4 in the high-temperature
    approximation)
Z = np.sum([np.exp(-E/(k*T)) for E in [E1, E2, E3, E4]])

print("Z: ", Z)

p1 = np.exp(-E1/(k*T))/Z
p2 = np.exp(-E2/(k*T))/Z

print("p1: ", p1)
print("p2: ", p2)

pThermal = [np.exp(-E/(k*T))/Z for E in [E1, E2, E3, E4]]

pInit = pThermal

def popChangesOverhauser(t, pops):
    p1 = pops[0]
    p2 = pops[1]
    p3 = pops[2]
    p4 = pops[3]


    # from eqs 4.11 and 4.18 we have
    # Bij = Wij / Wji
    # so B12 = W12 / W21

    W12 = 1000
    W21 = W12/B12
    W34 = 1000
    W43 = W34/B34

    W14 = 1000
    W41 = W14/B14

    We = 100000

    # use We2 if saturating both transitions
    We2 = 0

    return [p2*W21 - p1*W12 + p4*W41 - p1*W14 + (p2 - p1)*We,
             -p2*W21 + p1*W12 - (p2-p1)*We,
             p4*W43 - p3*W34 + (p4 - p3)*We2,
             p1*W14 + p3*W34 - p4*W43 - p4*W41 - (p4-p3)*We2]

timeSpan = [0,0.1] # from 0 to 0.1 s
sol = solve_ivp(popChangesOverhauser, timeSpan, pInit)


plt.plot(sol.t, sol.y[0], label = "$p_1$")
plt.plot(sol.t, sol.y[1], label = "$p_2$")
plt.plot(sol.t, sol.y[2], label = "$p_3$")
```

```
plt.plot(sol.t, sol.y[3], label = "$p_4$")
plt.legend()
plt.xlim(0, 0.02)
```

4.7 Exercises

1. Calculate the nuclear polarization enhancement for the solid effect and positive DNP in the limit that W_e completely saturates the $|1\rangle \leftrightarrow |4\rangle$ transition. On what time scale will this enhancement be established?
2. The typical polarization "buildup" time for the solid effect and ^{13}C in pyruvic acid is of the order of 30 min. Can you guess why?
3. The dynamics of a system of linear, first order differential equations may always be described by a set of orthogonal eigenmodes, as we will see in the next lecture. Mathematically, this problem is very close to solving the Schrödinger Equation - the key task is to find the eigenvectors and eigenvalues of the coupling matrix $\mathcal{M}$ with

$$\frac{\mathrm{d}\boldsymbol{p}}{\mathrm{d}t} = \mathcal{M}\boldsymbol{p} \tag{4.40}$$

   where $\boldsymbol{p}$ is the vector of populations.
   Since we cannot give analytic expressions for the eigenvalues for the system of Equations given by (4.4 - 4.7), we might as well use a computer to solve the initial value problem.
   In the code example above, this is shown for the Overhauser effect. Copy the code example and run it on your computer (take care with the indentations). Plot the nuclear spin polarization as a function of time.
   Next, do the same analysis for the solid effect. First write down the differential equations, and then implement a function `popChangesSolidEffect`. Solve it for a solid effect at 3 Tesla and 1 Kelvin, assuming an electron T_1 of the order of 100 ms.

DNP II. Spin Temperature | 5

5.1 The Main Ideas

In the previous lecture, we have seen how DNP mechanisms such as the solid effect or triple spin flips may be used to transfer polarization from electron to nuclear spins.

The observables in NMR and EPR however measure bulk properties, such as the bulk nuclear spin polarization of a given nuclear species. An intuitive and very useful concept to rationalize the evolution of these quantities is that of *spin temperature* [29]. We can think of the DNP process as cooling nuclear spins in the vicinity of the radical. We then want to know *how* efficient this cooling is, and *how* the cold is spread across the entire sample.

In this lecture, we will learn

- how the polarization can be expressed as a spin temperature
- how relaxation can then be thought of as a heat exchange with the lattice
- how to calculate the heat capacities of nuclear spins
- how hetero-nuclear heat exchange transfers polarization from one nuclear spin species to another
- how spin diffusion distributes heat across the sample

At the end of this lecture, you will have a framework with which you can rationalize the time course of DNP experiments.

5.2 The Concept of Spin Temperature

In the very first lecture, we have seen that the equilibrium temperature is given by

$$P_{\mathrm{eq}} = \tanh\left(\frac{\hbar\gamma B}{2kT}\right) \approx \frac{\hbar\gamma B}{2kT} \tag{5.1}$$

where the approximation holds in the high temperature limit $kT \gg \hbar\gamma B$. The temperature is the temperature of the sample, which is also referred to as the "lattice" temperature.

Now, if we have an arbitrary polarization $P \neq P_{\mathrm{eq}}$, then, we can solve Eq. 1 and describe the polarization with a temperature:

$$\frac{\hbar}{kT} =: \beta = \frac{2}{\gamma B}\,\mathrm{atanh}(P), \tag{5.2}$$

where we have defined the so-called *inverse temperature* β. Note that with this definition it is perfectly normal to have negative temperatures. Also, we have $\mathrm{atanh}(P) \to \infty$ for $P \to 1$, $\mathrm{atanh}(0) = 0$ and $\mathrm{atanh}(P) \to -\infty$ for $P \to 1$. Therefore, β is a continuous function of P in the interval $(-1, 1)$.

What is the spin temperature in thermal equilibrium? What happens with the spin temperature when the spins are first equilibrated at a specific temperature and field, and the field is then (i) increased or (ii) decreased?

Now on its own, this definition is, as Abragam and Proctor put it *perfectly straightforward, but also perfectly trivial* [30]. A key feature of the spin temperature approach is that it permits us to model the exchange between different spin systems as an exchange of heat. Before we look at that, we will have a look at the heat exchange of a few buckets of water.

[30]: Abragam et al. (1958), 'Spin Temperature'

5.3 Thermal Mixing of Some Buckets

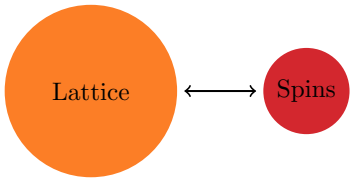

Figure 5.1: Thermal Mixing of Nuclear Spins with the lattice. The drawing is not to scale: The heat capacity of the lattice is far bigger than that of the nuclear spins. In this drawing the nuclear spins are red hot, i.e. their temperature is above the lattice temperature.

In magnetic resonance we always have one very big bucket, which is called the lattice. For practical purposes, this is just the sample temperature, and whatever we do to the spins has a negligible influence on the lattice temperature. This situation is shown in Fig. 5.1, and akin to lowering a cup containing a hot or cold drink into a bath tup at ambient temperature: eventually the cups content will assume the temperature of the bath tub.

If we assume that the heat exchange will occur at a given rate, then the change in spin temperature of the spins will be given by

$$\frac{\partial \beta_S}{\partial t} = -\frac{\beta_S - \beta_L}{\tau} \tag{5.3}$$

At this point, it is convenient to introduce a new variable $\beta'_S = \beta_S - \beta_L$. Then we can rewrite the above equation as

$$\frac{\partial \beta'_S}{\partial t} = -\frac{\beta'_S}{\tau} \tag{5.4}$$

Solving this differential equation by separation of variables gives exactly the mono-exponential relaxation that we see in many NMR experiments.

Now, if we have multiple spin species than in many cases nothing much changes. All spin species couple to the lattice, but because the lattice always stays at the sample temperature, there is no exchange between the spin species. If we have two spin species S and I, then we may write

ation as

$$\frac{\partial \beta'_S}{\partial t} = -\frac{\beta'_S}{\tau_S}\frac{\partial \beta'_I}{\partial t} = -\frac{\beta'_I}{\tau_I} \tag{5.5}$$

Note that τ_S and τ_I need not be equal, but otherwise nothing too interesting happens.

This does however change, if we allow a direct coupling between different spin species.

5.4 Hetero-Nuclear Thermal Mixing

Consider the setting in Fig. 5.3. Now we have introduced a second nuclear spin species and a *direct* coupling between the nuclear spins. For now, we will not worry about the origin of this coupling, but simply state that - in the absence of electron spins - it is usually negligible at high fields, but may become very important at low fields. Of course if the hetero-nuclear coupling is weak compared to the nuclear couplings to the lattice, nothing much happens.

But what if the hetero-nuclear coupling is strong? Then there will be an equilibration of the two reservoirs with each other, and the slower equilibration with the lattice will happen only at later times. Now the nuclear spin reservoirs do not have to differ tremendously in size, so there will be a change in temperatures of both reservoirs. To calculate this change, we then need to know the *size* of the reservoirs. This is known as the heat capacity.

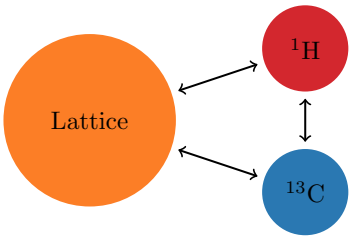

Figure 5.2: By introducing a second nuclear spin species, we can get more interesting dynamics if we allow for direct contact between the nuclear spins.

In classical physics, the heat capacity is the derivative of energy with respect to temperature. The energy is just the expectation value of the Hamiltonian, so for N spins, we have

$$\langle E \rangle = \langle \mathcal{H} \rangle = -\sum_{i=1}^{N} \gamma B \left\langle \hat{I}_z \right\rangle \tag{5.6}$$

$$= -N\gamma BIP \tag{5.7}$$

where we have inserted the result for $\left\langle \hat{I}_z \right\rangle$ from the first lecture. Note that we keep with the magnetic resonance convention of expressing energies in angular frequencies. Now in the high-temperature approximation we derived in the first lecture that

$$P \approx \frac{\hbar\gamma B}{kT}\frac{(I+1)}{3} = \beta\gamma B\frac{(I+1)}{3}, \tag{5.8}$$

Therefore we ahve

$$\langle E \rangle \approx -N\gamma^2 B^2 \beta \frac{I(I+1)}{3}, \tag{5.9}$$

and

$$C = \frac{\partial E}{\partial \beta} = -N\gamma^2 B^2 \frac{I(I+1)}{3} \tag{5.10}$$

Note that Goldman [29] uses a different sign convention for the heat capacity. Note furthermore, that to get the energy, we have used the absolute number of spins N. We could also use the concentration of spins, in which case C would be a *heat capacity density*. The advantage of the latter approach is that one can give material specific values. Either choice is fine, but of course we have to be consistent.

[29]: Goldman (1970), *Spin Temperature and Nuclear Magnetic Resonance in Solids*

As an example, let us consider the thermal mixing experiment in LiF by Abragam and Proctor [30]. Here, ^{7}Li has a natural abundance of 92.5 %, is spin 3/2 and has a gyromagnetic ratio of $\gamma_{\text{Li}} = 1.04\text{e}8\frac{\text{rad}}{\text{s T}}$. Fluorine on the other hand has an abundance of 100 %, is spin 1/2, and has $\gamma_{\text{F}} = 2.52\text{e}8\frac{\text{rad}}{\text{s T}}$.

[30]: Abragam et al. (1958), 'Spin Temperature'

For this system, the total energy in thermal equilibrium is

$$E = \beta \frac{B}{3} N \left(0.925 \gamma_{\mathrm{Li}}^2 \frac{15}{4} + 1 \gamma_{\mathrm{F}}^2 \frac{3}{4} \right) \tag{5.11}$$

Now if we saturate one nuclear species, we set its $\beta = 0$. Then, latter we may distribute the total energy over both species. Let us for example saturate the fluorine spin, and then have the two reservoirs mix. We find

$$\frac{\beta_{\mathrm{after}}}{\beta_{\mathrm{before}}} = \frac{0.925 \gamma_{\mathrm{Li}}^2 \frac{15}{4}}{0.925 \gamma_{\mathrm{Li}}^2 \frac{15}{4} + 1 \gamma_{\mathrm{F}}^2 \frac{3}{4}} = 0.44 \tag{5.12}$$

This means that if we saturate fluorine at high field, then allow for thermal mixing with lithium at low field, and afterwards observe again at high field, we should get a bit more than 40 % of the initial signal. This experiment has been carried out by Abragam and Proctor, and they found very good agreement, although they consistently got a little less signal. We will see why that is in a moment, but first we want to look at the dynamics of the system.

The evolution of the fluorine and lithium spins may be described by two coupled linear differential equations. We now drop the prime symbol, and all inverse temperatures β are referenced with respect to the lattice temperature.

$$\frac{\partial \beta_S}{\partial t} = -\frac{\beta_S}{\tau_S} - \frac{\beta_S - \beta_I}{\tau_{SI}} \tag{5.13}$$

$$\frac{\partial \beta_I}{\partial t} = -\frac{\beta_I}{\tau_I} + \frac{C_S}{C_I} \frac{\beta_S - \beta_I}{\tau_{SI}} \tag{5.14}$$

Note that here we have chosen to reference all heat exchange processes with respect to the S reservoir. If the S reservoir has larger heat capacity than the I reservoir, a transfer of heat from the S reservoir to the I reservoir will lead to a larger temperature change in the I reservoir. This is taken into account by the factor C_S/C_I in the second equation. Of course we could also have referenced everything to the I spins, in which case the inverse factor C_I/C_S would appear in the first equation, and τ_{SI} would take a different value accordingly. We therefore see that the value for τ_{SI} depends on the reference reservoir.

We may rewrite the equations (5.13)-(5.14) as

$$\frac{\partial \beta_S}{\partial t} = \beta_S \left(-\frac{1}{\tau_S} - \frac{1}{\tau_{SI}} \right) + \beta_I \frac{1}{\tau_{SI}} \tag{5.15}$$

$$\frac{\partial \beta_I}{\partial t} = \beta_I \left(-\frac{1}{\tau_I} - \frac{C_S}{C_I} \frac{1}{\tau_{SI}} \right) + \beta_S \frac{C_S}{C_I} \frac{1}{\tau_{SI}} \tag{5.16}$$

Then we can write them elegantly in matrix form

$$\dot{\vec{\beta}} = \boldsymbol{M} \vec{\beta} = \begin{pmatrix} -\frac{1}{\tau_S} - \frac{1}{\tau_{SI}} & \frac{1}{\tau_{SI}} \\ \frac{C_S}{C_I} \frac{1}{\tau_{SI}} & -\frac{1}{\tau_I} - \frac{C_S}{C_I} \frac{1}{\tau_{SI}} \end{pmatrix} \begin{pmatrix} \beta_S \\ \beta_I \end{pmatrix} \tag{5.17}$$

Now in complete analogy to lecture 2, we may calculate the eigenvalues λ_i and eigenvectors $\vec{v}_i$ of the matrix $\boldsymbol{M}$. The general solution is then given

by

$$\vec{\beta}(t) = \sum_{i=1}^{2} c_i \vec{v}_i \exp(+\lambda_i t), \tag{5.18}$$

where the c_i depend on the inital conditions.

To determine the c_i from the initial conditions, note that

$$\vec{\beta}(0) = \sum_i c_i \vec{v}_i = (\vec{v}_1, \vec{v}_2) \cdot \begin{pmatrix} c_1 \\ c_2 \end{pmatrix}. \tag{5.19}$$

Here $\mathscr{E} = (\vec{v}_1, \vec{v}_2)$ is a matrix of eigenvectors. Therefore we just need to calculate

$$\mathscr{E}^{-1}\vec{\beta} = \mathscr{E}^{-1}\mathscr{E}\begin{pmatrix} c_1 \\ c_2 \end{pmatrix} = \begin{pmatrix} c_1 \\ c_2 \end{pmatrix}, \tag{5.20}$$

to get the values for c_i for specific initial conditions.

Since in this case we do not need the eigenvalues, we may also use a computer and calculate the solution directly using

$$\vec{\beta}(t) = \exp(\boldsymbol{M}t)\beta(0). \tag{5.21}$$

This approach is subject of one of the exercises.

Brute-Force Hyperpolarization and Thermal Mixing

In lecture 1 we have discussed brute-force hyperpolarization, where nuclei are polarized simply bykeeping them at a high magnetic field and low temperatures for long times. While the proton T_1 is long, it still permits to get an acceptable polarization in a reasonable time. The same cannot be said for the carbon T_1. Then, one may polarize the proton spins only, and use thermal mixing at low fields, to transfer the polarization from proton to carbon spins [31].

[31]: Peat et al. (2016), 'Low-field thermal mixing in [1-13C] pyruvic acid for brute-force hyperpolarization'

5.5 The Origin of Spin Temperature and the Non-Zeeman Reservoir

The spin temperature model as we have used it above works with heat capacitys of well-defined reservoirs, for example the ^{7}Li and the ^{19}F reservoirs in LiF. This model works because each nuclear spin system always achieves an internal equilibrium on a fast time scale, namely the time scale of T_2. After this, the system may be described by a spin temperature β. But because T_2 is much faster than T_1, the energy of the system does not change significantly in short times. In fact, if we were to neglect the lattice, the energy would be completely constant.

In quantum mechanis, the expectation value of observables that commute with the Hamiltonian is *constant*. Since the ^{7}Li and ^{19}F Zeeman terms commute, they are each conserved on a timescale $< T_1$. There may well be significant other terms that commute with the Zeeman terms. These terms have non-zero expectation values for their energies, and accordingly, they also exhibit a heat capacity. This heat capacity is referred to as the *Non-Zeeman* heat capacity. The most prominent one is the truncated

dipolar interaction, arising from terms $\hat{A}$ and $\hat{B}$ in lecture 3. For crystals it is possible to calculate the expectation value of the dipolar interaction, using the method of moments [6]. One may think of the dipolar energy as arising from the interaction of one spin with a *local field* H_L due to the interacting second spin.

The heat capacity of the Non-Zeeman reservoir (which in the absence of other interactions is equal to the dipolar reservoir) may then be written in analogy to Equation (5.10) as

$$C_{NZ} = \gamma_S^2 H_L^2 N \frac{S(S+1)}{3} \tag{5.22}$$

In the case of purely dipolar interactions, it can be shwon that $\gamma_S^2 H_L^2 = (5/3)M_2$, where M_2 is the second moment of the spin-spin spectrum [29]. [1] The spin-spin spectrum is just the observed spectrum if this is dominated by dipolar interactions.

Note that the local field and hence the Non-Zeeman heat capacity are independent of the applied field, in contrast to the heat capacity of the Zeeman reservoir, which grows quadratically with increasing field.

The nuclear Non-Zeeman reservoir is important for thermal mixing between hetero-nuclei. This process becomes very efficient, when the magnetic field is reduced to values where the Zeeman interaction approximates the strength of the dipolar interaction (typically 10s of kHz).

The electron Non-Zeeman reservoir however can have a much larger second moment, since electron dipolar interactions can be much stronger than nuclear dipolar interactions. As a result, nuclei may exchange energy with the electron Non-Zeeman reservoir at fields as we use them for DNP experiments.

1: The n-th moment of a normalized spectrum $S(\omega)$ is simply $\int_{-\infty}^{\infty}(\omega - \omega_0)^n S(\omega)\mathrm{d}\omega$.

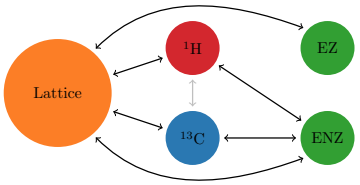

Figure 5.3: Introducing electron spins into the sample introduces another two reservoirs: The electron Zeeman reservoir and the electron Non-Zeeman reservoir. Note that we ignore the nuclear Non-Zeeman reservoirs due to their typically negligible influence on the other reservoirs. At intermediate fields the direct coupling between the proton and carbon reservoirs is negligible. However, they may still exchange heat via the electron Non-Zeeman reservoir. Note also that the electron Zeeman reservoir does not couple to any of the other reservoirs.

[32]: Cox et al. (1973), 'The Coupling of Two Nuclear Zeeman Reservoirs By the Electronic Spin-Spin Reservoir'

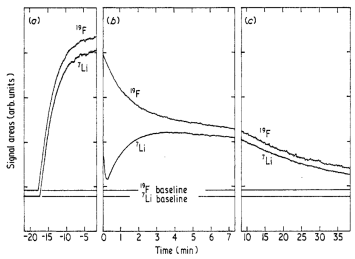

Figure 5.4: The thermal mixing experiment conducted by Cox, Bouffard and Goldman. In the first stage (a), both nuclear species are hyperpolarized using DNP. Then, (b) the lithium spins are saturated. However, they achieve an internal thermal equilibrium again on a timescale shorter than T_1. Finally, in (c) both spins relax to the lattice temperature.

5.6 Electron-Nuclear Thermal Mixing

By introducing electron spins into the sample, we add an electron Zeeman term to the Hamiltonian, but also a term for the electron-electron dipolar interactions. This term will come with a heat capacity, and the corresponding reservoir can exchange heat with nuclear spins. The microsopic processes that supports this heat exchange are just the triple-spin-flips that we have seen in the last lecture. We will refer to the corresponding heat exchange rate as *triple-spin-flip-heat-rate* rate (TSFHR).

The role of the ENZ reservoir as a link between different nuclear reservoirs was first shown by Cox et al. [32]. They used the LiF sample that we discussed previously, but doped it with F centres by irradiating the crystal with an electron beam. They hyperpolarized both ^{19}F and ^{7}Li using DNP at 2.5 Tesla and 0.74 K. Then they saturated the ^{7}Li spins, before allowing all spins to relax. The polarization or temperature of both the ^{7}Li and the ^{19}F were measured throughout the process using small flip angle pulses.

The process may be described with a set of three coupled differential equations.

5.7 Electron-Nuclear Thermal Mixing with Microwave Irradiation

Now that we have seen how we can equilibrate nuclear spins with the electron Non-Zeeman reservoir, we only need a way to *cool* the electron Non-Zeeman reservoir.

In this case it was Provotorov [33, 34] who showed that it is possible to cool the Non-Zeeman reservoir by heating the electron Zeeman reservoir using microwave irradiation. Of course Provotorov's idea was as upsetting to his colleagues as Overhauser's idea was to Overhauser's colleagues a few years earlier. Thankfully, Abragam met Provotorov on a trip to Russia and immediately realized the significance of Provotorov's work.

[33]: Provotorov (1961), 'Magnetic Resonance Saturation in Crystals'
[34]: Provotorov (1962), 'A Quantum-Statistical Theory of Cross Relaxation'

The derivation of the Provotorov equations is technical and given in full by Abragam and Goldman [35].

[35]: Abragam et al. (1982), 'Nuclear Magnetism: Order and Disorder'

Provotorov's idea is that when we apply a microwave field with a frequency *below* the electron resonance frequency, then we can still cause an electron flip, if the missing energy can be provided by the Non-Zeeman reservoir. This exchange of energy between the (rotating-frame) Zeeman reservoir and the Non-Zeeman reservoir conserves the total energy of both reservoirs, i.e.

$$\frac{\partial}{\partial t}\left(\Delta^2\beta_Z + D^2\beta_{NZ}\right) = \Delta^2\frac{\partial\beta_Z}{\partial t} + D^2\frac{\partial\beta_{NZ}}{\partial t} = 0, \tag{5.23}$$

where Δ is the Larmor frequency in the frame rotating at the microwave frequency (i.e. the resonance offset), and the frequency D characterizes the dipolar reservoir.

One may show that the expectation value for $\hat{I}_z$ in the *rotating frame* is

$$\left\langle \hat{I}_z \right\rangle = -\Delta \mathrm{Tr}\{\hat{I}_z^2\}\beta_Z \tag{5.24}$$

The change in $\hat{I}_z$ then is

$$\frac{\partial}{\partial t}\left\langle \hat{I}_z \right\rangle = -\Delta \mathrm{Tr}\{\hat{I}_z^2\}\frac{\partial\beta_Z}{\partial t}. \tag{5.25}$$

At the same time, we know that the change in $\hat{I}_z$ is due to the microwave field:

$$\frac{\partial}{\partial t}\left\langle \hat{I}_z \right\rangle = \omega_1 \left\langle \hat{I}_y \right\rangle \tag{5.26}$$

The expectation value of $\hat{I}_y$ may be obtained from a linear response treatment (see e.g. [35]):

[35]: Abragam et al. (1982), 'Nuclear Magnetism: Order and Disorder'

$$\left\langle \hat{I}_y(\Delta) \right\rangle = \mathrm{Tr}\hat{I}_x^2 \pi\omega_1(\Delta\alpha - \beta\Delta)g(\Delta) \tag{5.27}$$

We then use the fact that $\mathrm{Tr}\hat{I}_x^2 = \mathrm{Tr}\hat{I}_z^2$ (see, e.g., Slichter, Chapter (3) [6]) and obtain

$$\frac{\partial\beta_Z}{\partial t} = -\pi\omega_1^2\left(\beta_Z - \beta_{NZ}\right)g(\Delta) \tag{5.28}$$

Using Eq. (5.23), we get

$$\frac{\partial \beta_{NZ}}{\partial t} = \pi \omega_1^2 \frac{\Delta^2}{D^2} (\beta_Z - \beta_{NZ})\, g(\Delta) \tag{5.29}$$

These equations may be rewritten to include relaxation of the Zeeman and the Electron Non-Zeeman reservoir:

$$\frac{\partial \beta_Z}{\partial t} = -\pi \omega_1^2 (\beta_Z - \beta_{NZ})\, g(\Delta) - \frac{\beta_z}{T_1} \tag{5.30}$$

$$\frac{\partial \beta_{NZ}}{\partial t} = \pi \omega_1^2 \frac{\Delta^2}{D^2} (\beta_Z - \beta_{NZ})\, g(\Delta) - \frac{\beta_{NZ}}{T_{NZ}} \tag{5.31}$$

The linear differential equations 5.30, (5.31) are the Provotorov equations.

5.8 Spin Diffusion

Thus far we have assumed that all spins of a given spin species in a sample may - after a time T_2 - always be described by a single spin temperature. This assumption is not necessarily correct, and there are two impediments to achieving such equilibration.

5.8.1 The Diffusion Barrier

The first impediment to achieving a uniform temperature is the so-called diffusion barrier. The spins that are hyperpolarized by the electron spins are also very close to the electron spins. Accordingly, they have strong hyperfine couplings to the electrons. But due to these hyperfine couplings a flip-flop with a nucleus further away from the radical does not preserve energy anymore, and so such a flip-flop may occur at a substantially reduced rate, if at all.

Another feature of the strong hyperfine coupling is that it displaces the resonance frequency of the nuclear transition. As shown by Jannin and Stern et al. [36], this feature enables a direct observation of the diffusion barrier: After polarizing a sample with DNP, one may saturate the bulk spins using radio-frequency pulses. Following saturation, a part of the signal reappears. In the absence of other spins with a significant heat capacity, this reappearance may be attributed to diffusion from so-called core nuclei (which are close to the radical) to nuclei outside the diffusion barrier. In probing the diffusion barrier, this experimen therefore shows at the same time that the barrier is not insurmountable.

5.8.2 Bulk Spin Diffusion

Consider now the case where the radicals are relatively far apart. This is true in particular for hyperpolarizing substrates in which the radicals do not interact with the bulk of the polarized target molecule [37]. Then, one relies on bulk spin diffusion to transfer the polarization from the

source (i.e. the bulk) to the remote target locations. If there is a gradient in magnetization, then this will evolve according to the diffusion equation.

$$\frac{\partial \boldsymbol{M}(\boldsymbol{r},t)}{\partial t} = D\nabla^2 \boldsymbol{M}(\boldsymbol{r},t) \tag{5.32}$$

A typical value for the diffusion constant D of fluorine in CaF_2 is $10^{-12}\mathrm{cm}^2/\mathrm{s}$, where the Diffusion constant scales with γ^2 and the particle density $\sqrt{N}$. The time required to propagate magnetization by a distance r is

$$\tau = \frac{r^2}{D} \tag{5.33}$$

Diffusion therefore becomes exceedingly slow as the distances exceed 1 Micrometer. Note that for nuclei with a significant chemical shift anisotropy diffusion may slow down as the magnetic field is increased.

5.9 Concluding Remarks

The thermal mixing processes we have described uses a phenomenological approach - the heat exchange rate is simply determined from experiment. It is possible to calculate this (field-dependent) rate provided the EPR spin-spin spectrum and the (field-dependent) EPR spectrum are known. Vice versa, such an analysis may provide information about the spin-spin spectrum, and in particular about the degree of radical clustering.

5.10 Further Reading

- An accessible introduction to spin temperature has been given by Maurice Goldman in his book Spin Temperature and Nuclear Magnetic Resonance in Solids [29].
- Anatole Abragam and Maurice Goldman - Order and Disorder [35]
- Tom Wenckebach Essentials of Dynamic Nuclear Polarization [23]

[29]: Goldman (1970), *Spin Temperature and Nuclear Magnetic Resonance in Solids*

[35]: Abragam et al. (1982), 'Nuclear Magnetism: Order and Disorder'

[23]: Wenckebach (2016), *Essentials of Dynamic Nuclear Polarization*

5.11 Python

```
import matplotlib.pyplot as plt
import spindata
import numpy as np

tauS = 20
tauI = 10
tauSI = 0.1

gF = spindata.gamma("19F")
gLi = spindata.gamma("7Li")

cRatio = (gF**2*1*3*1)/(gLi**2*3*5*0.925) # 19F heat capacity (S)
    devided by 7Li heat capacity (I)

a = -1/tauS - 1/tauSI
```

```
b = 1/tauSI
c = cRatio*1/tauSI
d = - 1/tauI - cRatio*1/tauSI

T = a + d
D = a*d - b*c

lambda1 = T/2 + np.sqrt(T**2/4 - D)
lambda2 = T/2 - np.sqrt(T**2/4 - D)

print(lambda1)
print(lambda2)

ev1 = np.array([lambda1 - d, c])
ev2 = np.array([lambda2 - d, c])

print(ev1)
print(ev2)

# initial conditions
beta = np.array([0, 1])

cVals = np.linalg.inv(np.array([ev1, ev2]).T)@beta

# check that with the c_i s we indeed get the initial conditions
cVals[0]*ev1 + cVals[1]*ev2
```

5.12 Exercises

1. Thermal mixing in pyruvic acid. Pyruvate was the first substance for which the human metabolism could be tracked by MRI in vivo. The conventional strategy is to directly polarize the carbon spin of 1-^{13}C-pyruvic acid ($CH_3COCOOH$). Suppose that instead we polarize the proton spins to a polarization of 20 % at a field of 1 Tesla, and then allow for thermal mixing with the carbon spins at a lower field. Neglect all other reservoirs and the lattice, and use the high-temperature approximatino to estimate the maximum ^{13}C polarization if - prior to the mixing - the ^{13}C polarization is 0.
2. For more complicated systems with more than one reservoir, it is best to rely on a computer to find the eigenvalues and eigenvectors of the coupled differential equations. Implement a shorter version of the Python example given above, using `numpy`'s `np.linalg.eig` function. Plot the resulting spin temperatures.
3. Solve the initial value problem with the "brute-force" way. Copy the code from above to set up the matrix $\mathscr{M}$ and use `from scipy.linalg import expm` to propagate initial conditions.
4. Estimate the time to spread nuclear spin polarization accross (i) 1 Micrometer, and (ii) 1 Millimeter, for a diffusion constant of 10^{-12}cm^2/s. How

Quantum-Rotor- and Parahydrogen-induced Polarization

6

6.1 The Main Ideas

To this point we have studied dynamic nucleear polarization - where the large electron polarization is transferred to nuclear spins. Within this lecture we will not use electron spins at all. Instead, we will make use of the rotational interaction of freely rotating molecules.

For small molecules, this interaction brings about a splitting of the order of 10 or 10s of Kelvins, and so only the rotational ground state is populated at temperatures small compared to this splitting. This notion is of course only meaningful, if the molecules are free to rotate down to cryogenic temperatures. A populated rotor state would not by itself carry any spin polarization, if it were not for the *Pauli principle*. This principle simply states that for fermions the total wavefunction is antisymmetric, whereas for bosons it is symmetric. As a consequence, the symmetry of the rotational state dictates the symmetry of the spin state, or put more simply, only certain spin states are allowed with a given rotational state. Because the rotational splitting is much larger than the nuclear Zeeman interaction, the Pauli priniciple leads to very pure spin states at temperatures that are small compared to the rotational splitting. This situation is sketched graphically in Fig. 6.1.

We call the family of hyperpolarization techniques that exploit the rotational interaction of small molecules *Quantum-Rotor-Induced Polarization*. The vast majority of experimental techniques relies on parahydrogen (a linear top), and this chapter might equally have carried the title parahydrogen-induced polarization. There are however other molecules than hydrogen that display quantum-rotor-induced polarization, notably methyl groups and endofullerenes such as $H_2O@C_{60}$. Since we have studied the latter class in some detail, and since the methyl rotor is particularly simple to describe quantum-mechanically, we will disscuss both parahydrogen and the methyl rotor.

In this lecture, we will learn

- how the rotational interaction leads to a splitting in rotational states and how that splitting is reduced by a hindering potential
- how the Pauli principle enforces a subset of spin states for a given rotational state
- how the corresponding order is released in methyl groups via cross-relaxation
- how the corresponding order is released in hydrogen via hydrogenation reactions
- how signal-amplification by reversible exchange (SABRE) and side-arm hydrogenation (SAH) can extend the scope of parahydrogen-induced polarization.

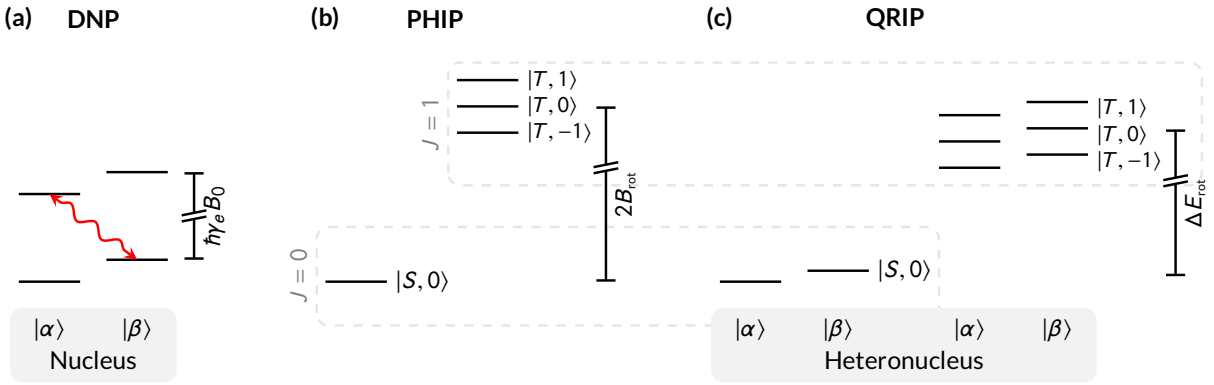

Figure 6.1: Hyperpolarization mechanisms. (a) In dynamic nuclear polarization, nuclear spins states are actively coupled to electron spin-states using microwave irradiation, as indicated by the red line. $|\alpha\rangle$ and $|\beta\rangle$ designate the spin state of the nucleus. (b) In parahydrogen induced polarization, the $J = 0$ state is associated with the nuclear singlet state, and the $J = 1$ state is associated with the nuclear triplet states, leading to a large splitting between these states. (c) In quantum-rotor-induced polarization, the situation is similar. The rotational splitting depends on the rotational Hamiltonian and may be reduced strongly if the rotation is hindered. In addition, a heteronucleus is required to release the spin order following a temperature jump. DNP = dynamic nuclear polarization; PHIP = parahydrogen induced polarization; QRIP = quantum-rotor-induced polarization. Figure copied from [38]

6.2 The Rotational Splitting

Both the methyl group and other quantum rotors are rotors, and their structure is described by a rotational Hamiltonian. A classical rigid body has three principal axes of rotation, and its energy is given by

$$E = \frac{1}{2}\omega_A I_A + \frac{1}{2}\omega_B I_B + \frac{1}{2}\omega_C I_C \tag{6.1}$$

where ω_A and I_A denote the angular frequency of the motion about axis A with moment of inertia I_A and so forth. The angular momentum along A is $L_A = \omega_A I_A$, and so the energy may be rewritten as

$$E = \frac{1}{2}\frac{L_A}{I_A} + \frac{1}{2}\frac{L_B}{I_B} + \frac{1}{2}\frac{L_C}{I_C} \tag{6.2}$$

So, in analogy, the Hamiltonian of a rigid quantum-rotor takes the form

$$\mathscr{H} = \frac{\hat{L}_A^2}{I_A} + \frac{\hat{L}_B^2}{I_B} + \frac{\hat{L}_C^2}{I_C} \tag{6.3}$$

For a spherical top, like CH_4, we have $I_A = I_B = I_C$.

For a symmetric top, we have $I_A = I_B \neq I_C$.

For a linear top, we have $I_A = I_B, I_C = 0$.

For an asymmetric top, we have $I_A < I_B < I_C$ (the ordering is a convention).

The tops above are discussed in standard textbooks on physical chemistry.

For a methyl group with a fixed axis of rotation, we have $I_A = I_B = 0 < I_C$.

6.2.1 The rotational splitting in methyl groups

The rotational splitting takes the most simple form in methyl groups that are free to rotate only about the symmetry axis of the methyl group. A substance in which this is realized is frozen γ-picoline, or 4-methyl-pyridine.

The rotational Hamiltonian may in this case be written, using only the z-component of the angular momentum operator in spherical coordinates [39]

$$\mathscr{H} = \frac{\hat{J}_z^2}{2I} + V(\phi) = -\frac{\hbar^2}{2I}\frac{\partial^2}{\partial\phi^2} + V(\phi) \tag{6.4}$$

Here $I = 5.3 \times 10^{-47}$ kg/m^2.

If the potential is zero, the eigenfunctions are

$$|m\rangle = \frac{1}{\sqrt{2\pi}} e^{im\phi} d\phi, \quad m = 0, \pm 1, \pm 2, \ldots. \tag{6.5}$$

These are normalized:

$$\int_0^{2\pi} \frac{1}{\sqrt{2\pi}} e^{-im\phi} \frac{1}{\sqrt{2\pi}} e^{im\phi} d\phi = 1. \tag{6.6}$$

The energies of the levels are

$$E_m = \frac{\hbar^2 m^2}{2I} \tag{6.7}$$

For a freely rotating methyl group, this splitting is of the order of a few Kelvin. In this limit, the rotational ground state may be populated strongly by equilibrating the sample at a temperature of less than a few Kelvin.

In most substances, methyl gropus do *not* rotate freely at temperatures of a few Kelvin. This effect may then be modelled by the potential term $V(\phi)$. The potential term which in its simplest form may be written as

$$V(\phi) = \frac{V_3}{2}\left[1 - \cos(3\phi)\right] \tag{6.8}$$

then mixes states with $n - m = \pm 3$, leading to new energy states, which in the limit of a strong barrier turn out to be triply degenerate. In this limit, the splitting between the first two states becomes zero [38, 40].

Shortly, we will see what consequences this has for the nuclear spin state, but first we will discuss the case of the hydrogen molecule.

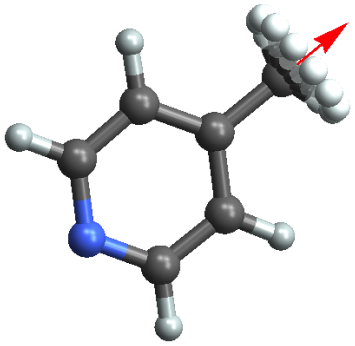

Figure 6.2: γ-picoline or 4-methyl-pyridine. In its solid form, the methyl group rotates freely even at cryogenic temperatures.

[38]: Meier (2018), 'Quantum-Rotor-Induced Polarization'
[40]: Horsewill (1999), 'Quantum Tunnelling Aspects of Methyl Group Rotation Studied By Nmr'

6.2.2 The rotational splitting of hydrogen

Molecular hydrogen, H_2 is a linear top. Rotation along the bond has zero moment of inertia, whereas rotations about two orthogonal axes perpendicular to the molecular bond have the same moment of inertia I. The Hamiltonian may therefore be written as

$$\mathscr{H} = \frac{\hat{L}_A^2 + \hat{L}_B^2}{2I} = \frac{\hat{\boldsymbol{L}}^2 - \hat{L}_C^2}{2I} \tag{6.9}$$

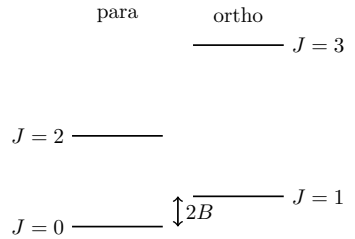

Figure 6.3: The rotational energy structure of hydrogen up to level $J = 3$. The degeneracy of the levels is $2J + 1$ (not shown). States with even J correspond to parahydrogen, those with odd J correspond to orthohydrogen.n

The energy levels are then [41]:

$$\mathscr{E} = \frac{\hbar^2 L(L+1)}{2I} = BL(L+1), \tag{6.10}$$

where we have introduced the rotational constant $B = \frac{\hbar^2}{2I}$. The bond length of hydrogen is 0.74 Å, and so the moment of inertia is $\sum mr^2 = 4.599 \times 10^{-48}$ kg m^2.

This leeds to a rotational constant of 88 Kelvin. So at temperatures of the order of 88 Kelvin or less, we will see a strong population of the rotational ground state.

6.3 The Pauli Principle

The Pauli Principle states that the wavefunction for fermions (half-integer spin particles, e.g. the proton) is antisymmetric with respect to the exchange of two particles, whereas that of bosons (integer spin particles, e.g. the deuterium nucleus) is symmetric with respect to the exchange of two particles. The wavefunction can always be written as a product of the space and spin parts:

$$|\Psi\rangle = \left|\Psi_{\text{space}}\right\rangle \otimes \left|\Psi_{\text{spin}}\right\rangle \tag{6.11}$$

Therefore, for the whole wavefunction to be antisymmetric, either the space- or the spin-part needs to be antisymmetric.

We will discuss the consequences of this principle first for hydrogen, and then for methyl groups.

6.3.1 Molecular Hydrogen

Let us consider the hydrogen molecule in more detail. This molecule comprises two magnetically equivalent spins with a J-coupling, and a dipolar coupling. It is for these couplings that the Hamiltonian is not diagonal in the Zeeman Product basis.

Instead, the eigenbasis of the spin part of molecular hydrogen is given by the so-called singlet state

$$|S\rangle = \frac{1}{\sqrt{2}}\left(|\alpha\beta\rangle - |\beta\alpha\rangle\right) \tag{6.12}$$

[11]: Levitt (2008), 'Spin Dynamics: Basics of Nuclear Magnetic Resonance'

and the three triplet states [11]:

$$|T_+\rangle = |\alpha\alpha\rangle \tag{6.13}$$

$$|T_0\rangle = \frac{1}{\sqrt{2}}\left(|\alpha\beta\rangle + |\beta\alpha\rangle\right) \tag{6.14}$$

$$|T_-\rangle = |\beta\beta\rangle \tag{6.15}$$

Note that the singlet state is *antisymmetric* - it changes sign under exchange of the two spin labels. The triplet states on the other hand are all symmetric - they do not change sign under exchange of the two spin labels.

Because the spatial part of the rotational ground state of water happens to be symmetric, the spin part needs to be antisymmetric to fullfill the Pauli principle. Hydrogen molecules with an antisymmetric spin part are known as *parahydrogen* and have even L. Those with a symmetric spin part are known as *orthohydrogen* and have odd L. The easiest way to enrich parahydrogen is to equilibrate hydrogen at very low temperatures. In order to achieve thermal equilibrium, one needs to temporarily break the equivalence or symmetry of the hydrogen molecule. This is done with a suitable catalyst, such as iron oxide.

Long-lived States

The singlet state of hydrogen has total spin 0, and does not give rise to an NMR signal. Orthowater on the other hand behaves as a spin-1 particle which readily gives an NMR signal. It is *not* possible to convert para- to orthohydrogen using RF pulse sequences. In fact, for isolated molecules, this conversion requires a symmetry breaking interaction. In the absence of such an interaction, any non-equilibrium population of ortho- and para-states is preserved indefinitely, and can give information about the temperature of the molecule at the time of formation. An intriguing example of this effect are ortho/parawater imbalances measured on comets [42].

[42]: Encrenaz (2008), 'Water in the Solar System'

If however one breaks the symmetry of the two spins forming the singlet state a tiny little bit, it is possible to convert singlet to triplet states and vice versa. The triplet-singlet-imbalance (TSI) may then still have a lifetime which is much longer than the longest T_1 in the system. Lifetimes of up to one hour have been measured on suitable prepared naphthalenes [43]. This offers possibilities in conjunction with hyperpolarization: Converting magnetization to a long-liged triplet-singlet-imbalance extends the time over which the hyperpolarization is usable [44].

[43]: Stevanato et al. (2015), 'A Nuclear Singlet Lifetime of More Than One Hour in Room-Temperature Solution'

For a review on the topic of long-lived states see for example [45].

[45]: Levitt (2012), 'Singlet Nuclear Magnetic Resonance'

6.3.2 Methyl

The methyl group has three protons, and so the spin states are three-spin states. Again, these are classified due to their symmetry, namely the symmetric A states:

$$|A, 3/2\rangle = |\alpha\alpha\alpha\rangle \tag{6.16}$$

$$|A, 1/2\rangle = \left(|\alpha\alpha\beta\rangle + |\alpha\beta\alpha\rangle + |\beta\alpha\alpha\rangle\right)/\sqrt{3} \tag{6.17}$$

$$|A, -1/2\rangle = \left(|\alpha\beta\beta\rangle + |\beta\alpha\beta\rangle + |\beta\beta\alpha\rangle\right)/\sqrt{3} \tag{6.18}$$

$$|A, -3/2\rangle = |\alpha\alpha\alpha\rangle \tag{6.19}$$

and the E_a states

$$|E_a, 1/2\rangle = \left(|\alpha\alpha\beta\rangle + \epsilon\,|\alpha\beta\alpha\rangle + \epsilon^*\,|\beta\alpha\alpha\rangle\right)/\sqrt{3} \tag{6.20}$$

$$|E_a, -1/2\rangle = \left(|\alpha\beta\beta\rangle + \epsilon\,|\beta\alpha\beta\rangle + \epsilon^*\,|\beta\beta\alpha\rangle\right)/\sqrt{3} \tag{6.21}$$

and the E_b states which are obtained from the E_a states with the substitution $\epsilon \leftrightarrow \epsilon^*$.

The E_a and E_b states acquire a phase factor ϵ^* and ϵ under cyclic permutation, respectively.

The rotational interaction splitts the states into the A states on the one hand, and the E_a and E_b states on the other. If a methyl group is able to rotate completely freely, this splitting is of the order of 6 Kelvin, and so equilibration at a temperature of 6 Kelvin or less will - compared to higher temperatures - lead to higher population of the A states.

6.4 Release of rotational spin order

To this point we have seen ways to create spin order, but none of these ways has resulted in magnetization. To actually record strong signals, we need cross-relaxation in the case of methyl, and a chemical reaction in the case of parahydrogen.

6.4.1 Methyl

Methyl groups don't like to react with anything. Here, a way to release the spin order at ambient temperature is via hetero-nuclear cross-relaxation. This happens, if the methyl group carries a ^{13}C hetero-nucleus. This effect has first been observed by Berger et al. [46] and an explanation has been given by Levitt et al. [47]. Similar effects have been observed in $H_2^{17}O@C_{60}$ [48].

[46]: Icker et al. (2012), 'Unexpected Multiplet Patterns Induced By the Haupt-Effect'

[47]: Meier et al. (2013), 'Long-Lived Nuclear Spin States in Methyl Groups and Quantum-Rotor-Induced Polarization'

[48]: Meier et al. (2018), 'Spin-Isomer Conversion of Water At Room Temperature and Quantum-Rotor-Induced Nuclear Polarization in the Water-Endofullerene $H_2O@C_{60}$'

6.4.2 Parahydrogen

Historically, the first hyperpolarization due to parahydrogen has been observed accidentally, and was (wronlgy) attributed to chemically induced dynamic nuclear polarization.

In Chemically Induced Dynamic Nuclear Polarization (CIDNP), a radical is formed by a chemical reaction. It turns out that the population of the radical energy levels may depend on the *nuclear* spin state. Together with a suitable relaxation mechanism, this may lead to strongly enhanced nuclear polarization [49].

In 1986, Bowers and Weitekamp predicted that the pure spin state of parahydrogen can be exploited to give strongly enhanced NMR signals, if the symmetry of parahydrogen is broken by means of a chemical reaction. Namely they suggested to hydrogenate an acetylene derivative of the form RC$\equiv$CR'. In this hydrogenation reaction, the two hydrogen atoms of a single hydrogen molecule are bond to the two carbons that share the acetylene (triple)-bond.

RC$\equiv$CR' + para-H_2

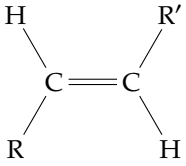

Figure 6.4: The chemical reaction suggested by Bowers and Weitekamp in their landmark 1986 paper.

[49]: Bowers et al. (1987), 'Parahydrogen and Synthesis Allow Dramatically Enhanced Nuclear Alignment'

In 1987 they demonstrated their predicted effect by hydrogenating the double bond of acrylonitrile (CH2$=$CH$-$C$\equiv$N) to form propionitrile (CH3$-$CH2$-$C$\equiv$N). They named the experiment PASADENA (Parahydrogen and Synthesis Allow Dramatically Enhanced Nuclear Alignment) [50].

In 1988, Pravica and Weitekamp demonstrated that somewhat different alignment effects are observed if the hydrogenation reaction is carried out at low fields (where chemical shift differences are not important), followed by a transport to and detection in a high-field magnet. Pravica

and Weitekamp named this effect ALTADENA (adiabatic longitudinal transport after dissociation engenders net alignment) [51].

Today, the family of ALTADENA and PASADENA experiments (and their descendants) is known as parahydrogen-induced polarization or PHIP.

As discussed by Natterer and Bargon [52] one can get a heuristic understanding of the mechanics of the PASADENA and ALTADENA experiments by considering the populations of a weakly coupled spin pair after the hydrogen reaction.

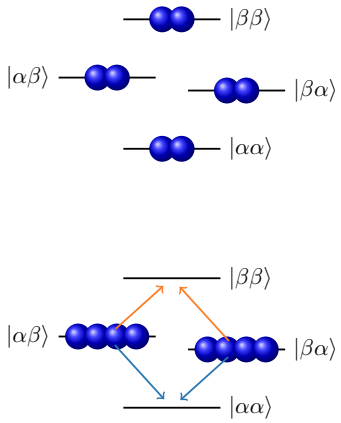

Figure 6.5: The PASADENA experiment. Compared to thermal equilibrium (top), the molecule derived from a reaction with parahydrogen has only the states $|\alpha\beta\rangle$ and $|\beta\alpha\rangle$ populated. This gives rise to strong positiv enhancements for the transitions involving the $|\beta\beta\rangle$ level, and to strong negative enhancements for transitions involving the $|\alpha\alpha\rangle$ level.

In the PASADENA experiment, the hydrogenation is carried out at *high* field. Then, if the resulting spin pair is weakly coupled (i.e. its J-coupling is weaker than the difference in chemical shift), it has the energy structure shown in Fig. 6.5. If the total nuclear spin of hydrogen is zero before the hydrogenation, then the total spin will also be zero after the hydrogen reaction. This means that the hydrogenation reaction will lead to a molecule in which only the states $|\alpha\beta\rangle$ and $|\beta\alpha\rangle$ are populated.

[52]: Natterer et al. (1997), 'Parahydrogen Induced Polarization'

In the ALTADENA experiment the hydrogenation reaction is carried out at low field. Even if the final hydrogen sites are chemically inequivalent, the singlet state is still a proper eigenstate. If the field is then increased (as the sample is moved into the magnet), the eigenstates change. If the change is slow enough, the populations will change with the states, and so only one of the resulting states will be populated. This effect is shown in 6.6.

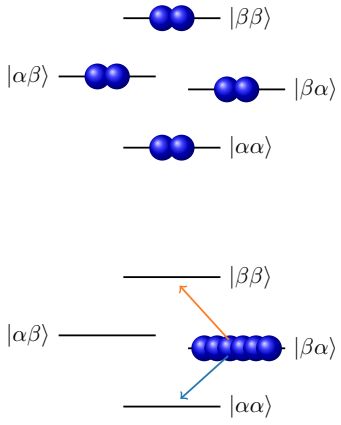

Figure 6.6: The ALTADENA experiment. Compared to thermal equilibrium (top), the molecule derived from a reaction with parahydrogen has only the singlet state populated. Upon transfer to high-field, this state evolves adiabatically into the $|\alpha\beta\rangle$ state, so that only this state is populated. This gives rise to strong positiv enhancements for the transitions involving the $|\beta\beta\rangle$ level, and to strong negative enhancements for transitions involving the $|\alpha\alpha\rangle$ level.

A sound analysis of the dynamics that occur in PASADENA and ALTADENA involves the spin density formalism.

The density operator of parahydrogen is

$$\rho = |\psi\rangle\langle\psi| = \frac{1}{2}\left(|\alpha\beta\rangle - |\beta\alpha\rangle\right)\left(\langle\alpha\beta| - \langle\alpha\beta|\right) \tag{6.22}$$

This expression may be rewritten using the vector notations

$$|\alpha\rangle = \begin{pmatrix}1\\0\end{pmatrix} \quad ; \quad |\beta\rangle = \begin{pmatrix}0\\1\end{pmatrix} \quad ; \tag{6.23}$$

as

$$\rho = \frac{1}{2}\left(\begin{pmatrix}1\\0\end{pmatrix}\otimes\begin{pmatrix}0\\1\end{pmatrix} - \begin{pmatrix}0\\1\end{pmatrix}\otimes\begin{pmatrix}1\\0\end{pmatrix} - \right)\otimes\left(\begin{pmatrix}1 & 0\end{pmatrix}\otimes\begin{pmatrix}0 & 1\end{pmatrix} - \begin{pmatrix}0 & 1\end{pmatrix}\otimes\begin{pmatrix}1 & 0\end{pmatrix}\right) \tag{6.24}$$

$$= \frac{1}{2}\left(\begin{pmatrix}0\\1\\0\\0\end{pmatrix} - \begin{pmatrix}0\\0\\1\\0\end{pmatrix}\right)\otimes\left(\begin{pmatrix}0 & 1 & 0 & 0\end{pmatrix} - \begin{pmatrix}0 & 0 & 1 & 0\end{pmatrix}\right) \tag{6.25}$$

$$= \frac{1}{2}\begin{pmatrix}0\\1\\-1\\0\end{pmatrix}\otimes\begin{pmatrix}0 & 1 & -1 & 0\end{pmatrix} \tag{6.26}$$

$$= \frac{1}{2}\begin{pmatrix}0 & 0 & 0 & 0\\0 & 1 & -1 & 0\\0 & -1 & 1 & 0\\0 & 0 & 0 & 0\end{pmatrix} \tag{6.27}$$

Using the matrix representations of two-spin spin operators that we calculated in the third lecture, we may rewrite this as

$$\rho = \frac{1}{4}\mathbf{1} - \hat{I}_{1x}\hat{I}_{2x} - \hat{I}_{1y}\hat{I}_{2y} - \hat{I}_{1z}\hat{I}_{2z} = \frac{1}{4}\mathbf{1} - \hat{\boldsymbol{I}}_1\hat{\boldsymbol{I}}_2 \tag{6.28}$$

6.4.3 SABRE

A severe limitation of the PHIP approach is that it is non-repeatable: the molecule is consumed in the hydrogenation step. The signal of the molecule may be enhanced, but only for a short time, and then the molecule is hydrogenated, and no further signal enhancement can be achieved.

In 2009 Simon Ducket and co-workers demonstrated that both parahydrogen and a substrate material may be bound revseribly to an irridium-based metal complex and thus enable a repeated polarization of the substrate molecule [53]. They named their method Signal Amplification by Reversible Exchange (SABRE). Today, SABRE enjoys widespread use in the PHIP community. For *in vivo* applications the (toxic) metal complex has to be removed from the solution, and an aqueous solution is required, whereas SABRE is conducted in organic solvents.

[53]: Adams et al. (2009), 'Reversible Interactions With Para-Hydrogen Enhance Nmr Sensitivity By Polarization Transfer'

6.4.4 SAH

Many molecules cannot be hyperpolarized with parahydrogen because they don't have unsaturated precursors, and they may also not bound to a metal complex. In such cases, parahydrogen may still play a role: In 2015, Francesca Reineri, Silvio Aime and co-workers introduced the concept of side-arm-hydrogenation (SAH) [54]. Here, an arm carrying an unsaturated bond is attached to the target substrate. The arm is hydrogenated, and the hyperpolarization is transfered to a site on the target either through an adiabatic change in field or through RF pulse sequences.

[54]: Reineri et al. (2015), 'Parahydrogen Induced Polarization of 13c Carboxylate Resonance in Acetate and Pyruvate'

6.5 Concluding Remarks

In this lecture we have seen a rather different hyperpolarization technique, PHIP. When should one use PHIP, and when should one use DNP?

The advantage of PHIP is that it is simple and economic in terms of instrumentation. Often a point is made that PHIP is orders of magnitude cheaper than DNP. This argument sounds compelling, but once staff costs and requirements for sterile operations in clinical settings are factored in, the difference in cost may not be so overwhelming anymore.

Perhaps more importantly, a PHIP experiment is typically done in seconds to minutes, whereas a bullet-or disslution-DNP experiment is done in 10s of minutes to hours. Arguably reserachers in PHIP have to fiddle less with their instrumentation, but they do need to know a bit more about chemistry.

Currently it looks as if parahydrogen may have the edge for metabolomic studies, where the use of organic solvents is acceptable. DNP on the other hand shines in combination with aqueous solvents and (for the time being) remains the more universal hyperpolarization tool, in particular with respect to physiological conditions.

6.6 Further Reading

- To learn more about the cross-relaxation mechanisms that determine the signal enhancement sin QRIP experiments, have a look at Jean-Nicolas Dumez's 2015 paper [55]
- For a review on parahydrogen-induced polarization see [52]
- For a more recent document including SABRE, and d-DNP as well, see [56].

[55]: Dumez et al. (2015), 'Theory of Long-Lived Nuclear Spin States in Methyl Groups and Quantum-Rotor Induced Polarisation'

[52]: Natterer et al. (1997), 'Parahydrogen Induced Polarization'

[56]: Kovtunov et al. (2018), 'Hyperpolarized Nmr Spectroscopy:d-Dnp, Phip, and Sabre Techniques'

6.7 Python

The code below allows you to plot the energy levels of a methyl group rotating along its axis in a three-fold potential V_3. Adapted from Ref. [38].

```
import numpy as np
import matplotlib.pyplot as plt

from scipy.constants import c, hbar, e

def wavenumbersToEV(x):
    return np.array(x)*hbar*c/e

I = 5.31e-47
V3 = 1e-3*e    # potential of one meV

# Setup Hamiltonian, energies in wavenumbers.
# The free rotor Hamiltonian in the free rotor basis
# has entries only on the diagonal.
# The code below creates the corresponding diagonal matrix.
maxN = 150
```

```
freeRotor = np.diag([hbar*n**2/(c*2*I) for n in range(int(-maxN/2
    + 1), int(maxN/2+1))])

# The potential term for the three-fold potential leads to entries
     on the
# - main diagonal
# - and on the off-diagonals shifted by +/- 3 positions (second/
    third lines)
potential3 = (2*np.identity(maxN)
             - np.diag(np.ones(maxN-3), 3)
             - np.diag(np.ones(maxN -3), -3))

potentialTerm = V3 / (4*hbar*c)*potential3

# now calculate eigenvalues for no potential, 10 mev, and 100 meV.
for scaleFactor in [0,10,100]:
    # the Hamiltonian is the sum of the free rotor Hamiltonian and
     the potential
    H = freeRotor + scaleFactor*potentialTerm

    # np.linalg.eig returns the eigenvalues or energies,
    # and the eigenvetors, or eigenstates
    energies, basisFunctions = np.linalg.eig(H)

    # now plot a sorted list of the eneriges to reveal the energy
    structure.
    plt.plot(wavenumbersToEV(sorted(energies)), "-x", label = "V3
    = {} meV".format(scaleFactor))

plt.xlim(0, 10)
plt.ylim(0, 0.04)
```

6.8 Exercises

1. Show that the expressions for singlet order in product operator form 6.28 and in matrix form 6.27 are identical by inserting the matrix representations for the spin operators.
2. Run the Python code for the example above. What is the degeneracy of the energy levels (i) for a free rotor and (ii) for a strongly hindered rotor?

Bibliography

Here are the references in citation order.

[1] Albert W. Overhauser. 'Polarization of Nuclei in Metals'. In: *Phys. Rev.* 92.2 (1953), pp. 411–415. DOI: 10.1103/physrev.92.411 (cited on page 4).

[2] T. R. Carver and C. P. Slichter. 'Polarization of Nuclear Spins in Metals'. In: *Physical Review* 92.1 (1953), pp. 212–213. DOI: 10.1103/physrev.92.212.2 (cited on page 4).

[3] Charles P. Slichter. 'The Discovery and Demonstration of Dynamic Nuclear Polarization-A Personal and Historical Account'. In: *Physical Chemistry Chemical Physics* 12.22 (2010), p. 5741. DOI: 10.1039/c003286g (cited on pages 4, 5).

[4] Matthew L. Hirsch et al. 'Brute-Force Hyperpolarization for NMR and MRI'. In: *Journal of the American Chemical Society* 137.26 (2015), pp. 8428–8434. DOI: 10.1021/jacs.5b01252 (cited on page 5).

[5] D.I Hoult and R.E Richards. 'The Signal-To-Noise Ratio of the Nuclear Magnetic Resonance Experiment'. In: *Journal of Magnetic Resonance (1969)* 24.1 (1976), pp. 71–85. DOI: 10.1016/0022-2364(76)90233-x (cited on page 8).

[6] Charles P. Slichter. 'Principles of Magnetic Resonance'. In: *Springer Series in Solid-State Sciences* (1990). DOI: 10.1007/978-3-662-09441-9 (cited on pages 9, 20, 31, 36, 50, 51).

[7] F.D Doty et al. 'Noise in High-Power, High-Frequency Double-Tuned Probes'. In: *Journal of Magnetic Resonance (1969)* 77.3 (1988), pp. 536–549. DOI: 10.1016/0022-2364(88)90011-x (cited on page 10).

[8] H. Nyquist. 'Thermal Agitation of Electric Charge in Conductors'. In: *Physical Review* 32.1 (1928), pp. 110–113. DOI: 10.1103/physrev.32.110 (cited on page 10).

[9] Helena Kovacs, Detlef Moskau, and Manfred Spraul. 'Cryogenically Cooled Probes-A Leap in Nmr Technology'. In: *Progress in Nuclear Magnetic Resonance Spectroscopy* 46.2-3 (2005), pp. 131–155. DOI: 10.1016/j.pnmrs.2005.03.001 (cited on page 10).

[10] Ēriks Kupče et al. 'Parallel Nuclear Magnetic Resonance Spectroscopy'. In: *Nature Reviews Methods Primers* 1.1 (2021), p. 27. DOI: 10.1038/s43586-021-00024-3 (cited on page 11).

[11] Malcolm H. Levitt. 'Spin Dynamics: Basics of Nuclear Magnetic Resonance'. In: (2008) (cited on pages 11, 18, 23, 58).

[12] Nate Silver. *The Signal and the Noise: Why So Many Predictions Fail-But Some Don't*. Penguin Press, 2013 (cited on page 11).

[13] Alexander G. Maryasov and Michael K. Bowman. 'Comment on "Modeling of Motional Epr Spectra Using Hindered Brownian Rotational Diffusion and the Stochastic Liouville Equation" [j. Chem. Phys. 152, 094103 (2020)]'. In: *The Journal of Chemical Physics* 153.2 (2020), p. 027101. DOI: 10.1063/5.0010661 (cited on pages 16, 30).

[14] A. Abragam and B. Bleaney. *Electron Paramagnetic Resonance of Transition Ions*. Clarendon Press, Oxford, 1970 (cited on pages 17, 23).

[15] Andreas Brinkmann and Malcolm H. Levitt. 'Symmetry Principles in the Nuclear Magnetic Resonance of Spinning Solids: Heteronuclear Recoupling By Generalized Hartmann-Hahn Sequences'. In: *The Journal of Chemical Physics* 115.1 (2001), pp. 357–384. DOI: 10.1063/1.1377031 (cited on pages 19, 23).

[16] Philipp K. Janert. *Data Analysis with Open Source Tools*. Sebastopol, CA 95472: O'Reilly, 2010 (cited on pages 20, 23).

[17] F Kurdzesau et al. 'Dynamic Nuclear Polarization of Small Labelled Molecules in Frozen Water-Alcohol Solutions'. In: *Journal of Physics D: Applied Physics* 41.15 (2008), p. 155506. DOI: 10.1088/0022-3727/41/15/155506 (cited on pages 22, 26).

[18] Lloyd Lumata et al. 'Electron Spin Resonance Studies of Trityl Ox063 At a Concentration Optimal for Dnp'. In: *Phys. Chem. Chem. Phys.* 15.24 (2013), p. 9800. DOI: 10.1039/c3cp50186h (cited on page 22).

[19] Andrea Capozzi et al. 'Efficient Hyperpolarization of U-13 C-Glucose Using Narrow-Line Uv-Generated Labile Free Radicals'. In: *Angewandte Chemie International Edition* 58.5 (2018), pp. 1334–1339. DOI: 10.1002/anie.201810522 (cited on page 22).

[20] Arthur Schweiger and Gunnar Jeschke. *Principles of pulse electron paramagnetic resonance*. Oxford University Press, 2005, nil (cited on pages 26, 30).

[21] Claude Cohen-Tannoudji, Bernard Diu, and Franck Laloe. *Quantum Mechanics*. John Wiley, 2005 (cited on page 26).

[22] Luca A Pardi et al. 'Multifrequency Epr Spectra of Molecular Oxygen in Solid Air'. In: *Journal of Magnetic Resonance* 146.2 (2000), pp. 375–378. DOI: 10.1006/jmre.2000.2175 (cited on page 32).

[23] W.T. Wenckebach. *Essentials of Dynamic Nuclear Polarization*. Spindrift Publications, 2016 (cited on pages 32, 41, 42, 53).

[24] Luciano Ramalho. *Fluent Python*. O'Reilly, 2015, nil (cited on page 33).

[25] Enrico Ravera, Claudio Luchinat, and Giacomo Parigi. 'Basic Facts and Perspectives of Overhauser DNP NMR'. In: *Journal of Magnetic Resonance* 264.nil (2016), pp. 78–87. DOI: 10.1016/j.jmr.2015.12.013 (cited on page 39).

[26] C. D. Jeffries. 'Polarization of Nuclei By Resonance Saturation in Paramagnetic Crystals'. In: *Phys. Rev.* 106.1 (1957), pp. 164–165. DOI: 10.1103/physrev.106.164 (cited on page 40).

[27] W.Th. Wenckebach. 'Dynamic Nuclear Polarization Via the Cross Effect and Thermal Mixing: A. The Role of Triple Spin Flips'. In: *Journal of Magnetic Resonance* 299.nil (2019), pp. 124–134. DOI: 10.1016/j.jmr.2018.12.018 (cited on page 42).

[28] W.Th. Wenckebach. 'Dynamic Nuclear Polarization Via the Cross Effect and Thermal Mixing: B. Energy Transport'. In: *Journal of Magnetic Resonance* 299.nil (2019), pp. 151–167. DOI: 10.1016/j.jmr.2018.12.020 (cited on page 42).

[29] Maurice Goldman. *Spin Temperature and Nuclear Magnetic Resonance in Solids*. Oxford University Press, 1970 (cited on pages 45, 47, 50, 53).

[30] A. Abragam and W. G. Proctor. 'Spin Temperature'. In: *Physical Review* 109.5 (1958), pp. 1441–1458. DOI: 10.1103/physrev.109.1441 (cited on pages 46, 47).

[31] David T. Peat et al. 'Low-field thermal mixing in [1-13C] pyruvic acid for brute-force hyperpolarization'. In: *Physical Chemistry Chemical Physics* 18.28 (2016), pp. 19173–19182. DOI: 10.1039/c6cp02853e (cited on page 49).

[32] S F J Cox, V Bouffard, and M Goldman. 'The Coupling of Two Nuclear Zeeman Reservoirs By the Electronic Spin-Spin Reservoir'. In: *Journal of Physics C: Solid State Physics* 6.5 (1973), pp. L100–L103. DOI: 10.1088/0022-3719/6/5/006 (cited on page 50).

[33] B.N. Provotorov. 'Magnetic Resonance Saturation in Crystals'. In: *Sov. Phys. JETP 14 (1962)* 14.5 (1961), pp. 1126–1131 (cited on page 51).

[34] B.N. Provotorov. 'A Quantum-Statistical Theory of Cross Relaxation'. In: *Sov. Phys. JETP 15 (1962)* 15.3 (1962), pp. 611–614 (cited on page 51).

[35] Anatole Abragam and Maurice Goldman. 'Nuclear Magnetism: Order and Disorder'. In: *The International Series of Monographs on Physics* (1982) (cited on pages 51, 53).

[36] Quentin Stern et al. 'Direct Observation of Hyperpolarization Breaking Through the Spin Diffusion Barrier'. In: *Science Advances* 7.18 (2021), nil. DOI: 10.1126/sciadv.abf5735 (cited on page 52).

[37] D. Gajan et al. 'Hybrid Polarizing Solids for Pure Hyperpolarized Liquids Through Dissolution Dynamic Nuclear Polarization'. In: *Proceedings of the National Academy of Sciences* 111.41 (2014), pp. 14693–14697. DOI: 10.1073/pnas.1407730111 (cited on page 52).

[38] Benno Meier. 'Quantum-Rotor-Induced Polarization'. In: *Magnetic Resonance in Chemistry* 56.7 (2018), pp. 610–618. DOI: 10.1002/mrc.4725 (cited on pages 56, 57, 63).

[39] Morris Edgar. Rose. *Elementary Theory of Angular Momentum*. New York: Dover Publications, 1995 (cited on page 57).

[40] A.J. Horsewill. 'Quantum Tunnelling Aspects of Methyl Group Rotation Studied By Nmr'. In: *Progress in Nuclear Magnetic Resonance Spectroscopy* 35.4 (Dec. 1999), pp. 359–389. DOI: 10.1016/s0079-6565(99)00016-3 (cited on page 57).

[41] Philip R. Bunker and Per Jensen. *Molecular Symmetry and Spectroscopy*. National Research Council of Canada, 2006 (cited on page 58).

[42] Thérèse Encrenaz. 'Water in the Solar System'. In: *Annual Review of Astronomy and Astrophysics* 46.1 (2008), pp. 57–87. DOI: 10.1146/annurev.astro.46.060407.145229 (cited on page 59).

[43] Gabriele Stevanato et al. 'A Nuclear Singlet Lifetime of More Than One Hour in Room-Temperature Solution'. In: *Angewandte Chemie International Edition* 54.12 (2015), pp. 3740–3743. DOI: 10.1002/anie.201411978 (cited on page 59).

[44] Stuart J. Elliott et al. 'Hyperpolarized Long-Lived Nuclear Spin States in Monodeuterated Methyl Groups'. In: *Physical Chemistry Chemical Physics* 20.1 (2018), p. 9755. DOI: 10.1039/c8cp00253c (cited on page 59).

[45] Malcolm H. Levitt. 'Singlet Nuclear Magnetic Resonance'. In: *Annu. Rev. Phys. Chem.* 63.1 (May 2012), pp. 89–105. DOI: 10.1146/annurev-physchem-032511-143724 (cited on page 59).

[46] Maik Icker and Stefan Berger. 'Unexpected Multiplet Patterns Induced By the Haupt-Effect'. In: *Journal of Magnetic Resonance* 219 (June 2012), pp. 1–3. DOI: 10.1016/j.jmr.2012.03.021 (cited on page 60).

[47] Benno Meier et al. 'Long-Lived Nuclear Spin States in Methyl Groups and Quantum-Rotor-Induced Polarization'. In: *J. Am. Chem. Soc.* 135.50 (2013), pp. 18746–18749. DOI: 10.1021/ja410432f (cited on page 60).

[48] Benno Meier et al. 'Spin-Isomer Conversion of Water At Room Temperature and Quantum-Rotor-Induced Nuclear Polarization in the Water-Endofullerene $H_2O@C_{60}$'. In: *Physical Review Letters* 120.26 (2018), p. 266001. DOI: 10.1103/physrevlett.120.266001 (cited on page 60).

[49] R. Kaptein and J.L. Oosterhoff. 'Chemically Induced Dynamic Nuclear Polarization Ii'. In: *Chemical Physics Letters* 4.4 (1969), pp. 195–197. DOI: 10.1016/0009-2614(69)80098-9 (cited on page 60).

[50] C. Russell Bowers and D. P. Weitekamp. 'Parahydrogen and Synthesis Allow Dramatically Enhanced Nuclear Alignment'. In: *Journal of the American Chemical Society* 109.18 (1987), pp. 5541–5542. DOI: 10.1021/ja00252a049 (cited on page 60).

[51] Michael G. Pravica and Daniel P. Weitekamp. 'Net Nmr Alignment By Adiabatic Transport of Parahydrogen Addition Products To High Magnetic Field'. In: *Chemical Physics Letters* 145.4 (1988), pp. 255–258. DOI: 10.1016/0009-2614(88)80002-2 (cited on page 61).

[52] Johannes Natterer and Joachim Bargon. 'Parahydrogen Induced Polarization'. In: *Progress in Nuclear Magnetic Resonance Spectroscopy* 31.4 (1997), pp. 293–315. DOI: 10.1016/s0079-6565(97)00007-1 (cited on pages 61, 63).

[53] R. W. Adams et al. 'Reversible Interactions With Para-Hydrogen Enhance Nmr Sensitivity By Polarization Transfer'. In: *Science* 323.5922 (2009), pp. 1708–1711. DOI: 10.1126/science.1168877 (cited on page 62).

[54] Francesca Reineri, Tommaso Boi, and Silvio Aime. 'Parahydrogen Induced Polarization of 13c Carboxylate Resonance in Acetate and Pyruvate'. In: *Nature Communications* 6.1 (2015), p. 5858. DOI: 10.1038/ncomms6858 (cited on page 62).

[55] Jean-Nicolas Dumez et al. 'Theory of Long-Lived Nuclear Spin States in Methyl Groups and Quantum-Rotor Induced Polarisation'. In: *The Journal of Chemical Physics* 142.4 (2015), p. 044506. DOI: 10.1063/1.4906273 (cited on page 63).

[56] Kirill V. Kovtunov et al. 'Hyperpolarized Nmr Spectroscopy:d-Dnp, Phip, and Sabre Techniques'. In: *Chemistry - An Asian Journal* 13.15 (2018), pp. 1857–1871. DOI: 10.1002/asia.201800551 (cited on page 63).

Abbreviations

DNP Dynamic Nuclear Polarization

PHIP Parahydrogen-induced polarization

QRIP Quantum-rotor-induced polarization

SEOP Spin-Exchange Optical Pumping

Alphabetical Index